THESIS FOR THE DEGREE OF LICENTIATE OF ENGINEERING IN THERMO
AND FLUID DYNAMICS

Numerical modelling of particulate matter deposition in exhaust gas after-treatment systems

ANANDA SUBRAMANI KANNAN

Numerical modelling of particulate matter deposition in exhaust gas after-treatment systems
ANANDA SUBRAMANI KANNAN

Numerical modelling of particulate matter deposition in exhaust gas after-treatment systems

ANANDA SUBRAMANI KANNAN
Department of Mechanics and Maritime Sciences
Chalmers University of Technology

ABSTRACT

As urban air quality declines, the corresponding levels of particulate matter (PM) such as sulfates, nitrates and black carbon rise, posing the greatest risks to human health. Hence, the control of these particulate emissions constitutes a major global challenge that commands serious attention. In order to design strategies to mitigate PM emissions, it is necessary to establish the physical laws that govern their motion and deposition at these nano-scales. These systems are challenging to understand particularly as both the decreased momentum exchange with the gas (rarefaction or non-continuum effects due to the small sizes) and the meandering Brownian particle trajectories need to be studied simultaneously. For such an effort, numerical methods offer an attractive alternative to experiments, as the costs of setting up complicated experiments can be offset by insilico-methods that can provide a more exhaustive description of the particulate flow physics.

In this work, we propose a suite of numerical tools that can be used for understanding PM deposition (including its transformation) in traditional after-treatment devices. First, we undertake a system level modelling of PM deposition in exhaust after-treatment devices, such as diesel particulate filters (DPF's), using a computational fluid dynamics driven approach. We show that the results from a fully Eulerian simulation of the the PM deposition process (based on the assumption of inertialess inert particles) shows lesser PM capture than actual experimental data. The noted disagreement can be attributed to the assumption of inert particles while modelling the deposition. Consequently, a multiphase direct numerical simulation (DNS) technique, that can handle the fluid scales as well as the inherent particle-fluid coupling, is identified as an alternative to model these reactive particulate flows. We formulate such a framework by coupling the extended Langevin description of the particle with a mirroring Immersed boundary method. Further, to get an accurate resolution of the particle dynamics, we solve for it using a finite element based rigid body solver. This entire technique (referred to as the IB-FSI framework) is implemented in the immersed boundary code `IPS IBOFlow` (developed by Fraunhoffer Chalmers centre). We analyse the consequences of resolving Brownian motion in an unbounded domain using this framework and evaluate the diffusion dynamics (mean squared displacements, velocity auto-correlation functions and diffusivities) of a spherical transported particle, in relation to the conventional Lagrangian Langevin treatment. Moreover, we demonstrate the applicability of such a method to resolve the Brownian dynamics of PM aerosols with particle densities comparable to a real soot-particle. We finally extend this framework to describe fractal like soot PM in unbounded domains.

Keywords: Brownian motion, DNS, Immersed boundary method, Nanoscales, PM transformation and Rarefied gas

To my son... My lucky charm...

LIST OF ABBREVIATIONS

Abbreviations

AMG   –   Algebraic multi-grid
CE   –   Capture efficiency
CFD   –   Computational Fluid Dynamics
DNS   –   Direct numerical simulation
DOC   –   Diesel oxidation catalyst
DeNOx –   Diesel Nitrous oxides (NOx) reduction catalyst
DPF   –   Diesel particulate filter
EC   –   European commission
ESPs   –   Electrostatic Precipitators
FEM   –   Finite element method
FSI   –   Fluid structure interaction
GPU   –   Graphical processing unit
HC   –   Hydrocarbon
IB   –   Immersed boundary
IBC   –   Immersed boundary condition
MSD   –   Mean squared displacement
ODE   –   Ordinary differential equation
PM   –   Particulate matter
SDE   –   Stochastic differential equation
SEM   –   Scanning electron microscope
TIS   –   Tanks in series
VOF   –   Volume of fluid

Thesis

This thesis consists of an extended summary and the following appended papers:

Paper A
Henrik Ström, Jonas Sjöblom, Ananda Subramani Kannan, Houman Ojagh, Oskar Sundborg, and Jan Koegler. Near-wall dispersion, deposition and transformation of particles in automotive exhaust gas aftertreatment systems. *International Journal of Heat and Fluid Flow* **70** (2018), 171 –180. ISSN: 0142-727X. DOI: `https://doi.org/10.1016/j.ijheatfluidflow.2018.02.013`

Paper B
Ananda Subramani Kannan, Vasileios Naserentin, Andreas Mark, Dario Maggiolo, Gaetano Sardina, Srdjan Sasic, and Henrik Ström. A novel multiphase DNS method for the resolution of Brownian motion of soot-like particles in a rarefied gas using a continuum framework. *To be submitted to a journal* (2018)

x

CONTENTS

Part I
Extended Summary

Chapter 1
Introduction

This chapter provides a general overview about particulate matter (PM) emissions and the need for their mitigation. The common sources of PM emissions are first discussed, followed by possible strategies for their mitigation. The need for in-silica based design and development strategies is addressed, along with a brief overview of our proposed method.

1.1 Particulate emissions: A general outlook

Urban air quality has been on the decline since the Industrial revolution, particularly due to the increasing energy demands for the modernization of our society. With the increasing dependence on fossil fuels, the corresponding levels of particulate matter (PM) such as PM10 (particle less than 10 microns in diameter) and PM2.5 (particles less than 2.5 microns in diameter), that contain pollutants such as sulpahtes and nitrates rise, posing the greatest risks to human health [63]. Emissions from households, industrial plants and road transport account for a majority of these fine aerosols (PM2.5 and PM10) that are emitted in Europe (c.f. Fig. 1.1). Hence, the European commission (EC) has implemented a series of Directives that establishes the health based standards and objectives for these pollutants (Directive 2008/50/EC of the European Parliament [16]). Stringent measures to control the emissions of PM (from the various sources) have to be adopted if these demands from the EC are to be met. Thus, there is a palpable need for strategies for PM mitigation.
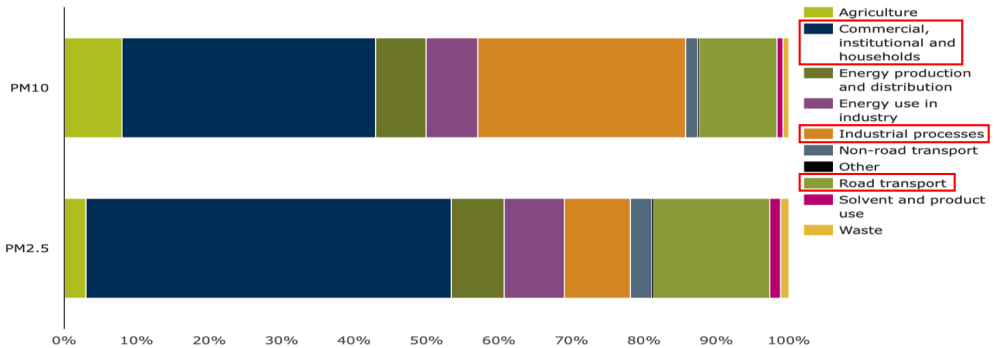
Figure 1.1: *Common sources of emissions for PM10 and PM2.5 (figure adapted from [58]).*

PM are usually formed due to incomplete combustion of hydrocarbon-based fuels during a variety of common combustion processes for power generation, vehicular propulsion etc. The widespread dispersion of these nanoscale particulates (aerosols) poses a significant

health hazard, particularly as these can directly settle in the human lung leading to severe breathing difficulties. There is thus a growing need to curb such emissions which would necessitate a deeper understanding of the underlying phenomena including the creation, growth and transformation of PM. In general, these aggregates are composed of fine primary particles (typical size range 10-20 nm) that coagulate to form irregular fractal-clusters (See Fig. 1.2) that have a broad size distribution (typically 80 - 500 nm) [2]. The physical laws governing the dispersion of such aggregates may differ from its macroscopic (continuum) counterpart in that molecular effects have a more pronounced effect.

The dimensions of the fractal-like aggregates are usually comparable with the mean free path of the surrounding gas they are dispersed in, which would mean that they will no longer experience a continuum but instead collide with the constitutive molecules or atoms. This results in two primary effects. Firstly, the regular collisions act as a random driving force on the particle maintaining an incessant irregular motion and secondly, they give rise to a frictional force (or drag) for a forced motion. The superposition of these two opposing effects (gives rise to a meandering motion commonly referred to as Brownian motion [19, 77]) drives the dispersion of PM and knowledge about these complex phenomena can be utilized to develop strategies for PM mitigation.
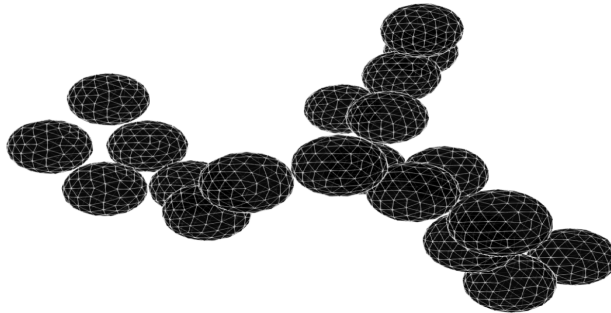
Figure 1.2: *A typical fractal-like soot aggregate.*

1.2   Some strategies for mitigating PM emissions

The most generic mitigation strategy is some form of after-treatment of the exhaust gases. For vehicular emissions, particularly diesel based propulsion, a combination of the diesel oxidation catalyst (DOC), diesel particulate filter (DPF) and diesel NOx reduction catalyst (DeNOx) are employed downstream from the tail pipe to regulate the exhaust. Note that the emphasis of this work is on PM mitigation (i.e. on the DPF) and a wall-flow monolith is the most common type of filtration element employed in such an application. Similar solutions are available for household and industrial exhaust as well (such as Electrostatic Precipitators (ESPs), Fabric filters etc.). Hence, the solutions proposed can be extended to these other exhaust treatment devices as well.
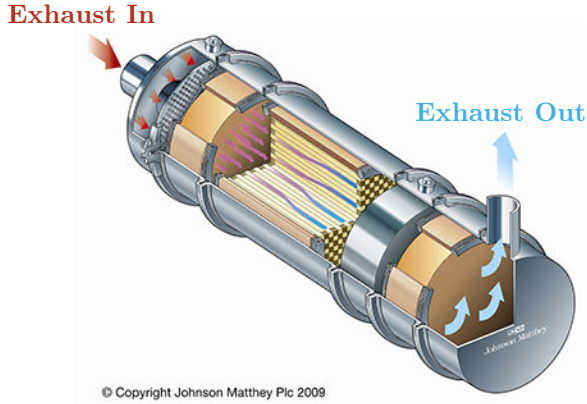
Figure 1.3: *An example of a PM emission mitigation device: Diesel particulate filter (DPF) employed in diesel powered drives.*

DPF's are routinely used today to mitigate PM emissions from vehicular exhausts (from both diesel and petrol engines). They are commonly made from cordierite or silicon carbide extruded monoliths (or substrates) in which every second channel is plugged in either end, creating a chessboard-like appearance of the monolith front and back c.f. Fig. 1.3. A second layer of porous material, called the wash coat, is deposited inside these monolith channels to maximize the surface area available for PM deposition (c.f. Fig. 1.4). The exhaust gas is only allowed to enter the channels which are open towards the inlet side, the so-called inlet channels. The gas is then forced to flow through the porous wall into the four adjacent outlet channels [45]. The channels have a general dimension with $O(mm)$, while the pore dimensions in the wash coat layer (where in the PM deposits) are in the $O(\mu m)$. Hence the relevant phenomena are typically in the micro-scales. Moreover, the flow in these channels is laminar (Reynolds numbers are of the order of a couple of hundreds), meaning that PM accumulates on the inside and on the porous walls of the inlet channel through Brownian deposition/diffusion and interception.
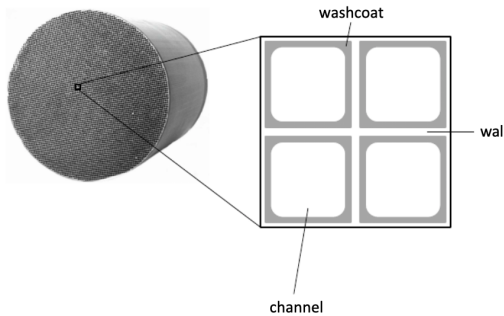
Figure 1.4: *Schematic of the entrance to four monolith channels. These channels have square cross-sections, which are rounded by the porous wash coat that maximizes the surface area available for PM deposition. Figure adapted from [79].*

4

Although effective at PM capture, these DPF's are associated with a significant fuel penalty, mainly because of the pressure built up due to deposition (i.e. the channels are clogged with PM). Hence, smarter technologies to circumvent the deficiencies of these traditional monolith filters are desirable. Moreover, a deeper understanding of the movement and deposition of the particulates under these challenging conditions, where both continuum and molecular effects drive the phenomena, would permit the creation of materials/devices that would allow for more environmentally friendly and energy-efficient (clean) transportation.

Thus, there is a need for methods that can provide a heuristic overview of the complex underlying Brownian dispersion phenomena that drives the deposition of the fine aerosols. This would ultimately contribute towards rapid design and prototyping of PM mitigation technologies. Numerical tools such as those based on the spatial and temporal resolution of the governing physics (for example the computational fluid dynamics (CFD) simulations of the fluid flow in the channels) or tools that can simultaneously solve for both the particle and fluid descriptions (for example multiphase direct numerical simulation (DNS) of particulate aerosols), can supplement complex trial and error based design strategies. Moreover, these numerical methods can probe regions inside the monolith channel that are traditionally harder to access through experimental measurement techniques. Hence in this work, we emphasize on the development of high fidelity numerical tools that can accurately model or resolve the necessary particulate flow (i.e. the motion of particles in the size range 80 nm to 1000 μm) to either supplement or complement traditional experimental prototyping based design strategies.

1.3   Aim

The transport of PM aerosols (in the size range 80 nm to 1000 μm) in traditional exhaust after-treatment devices (such as the monolith channels of a DPF) presents a challenging problem that couples both micro and macro-scale phenomena. Hence, in order to design the next generation of PM mitigation devices, the knowledge about such particulate flows needs to be deepened. Consequently, the main objective of the current work is to develop various strategies to numerically model or describe the PM deposition (including its transformation) in traditional mitigation devices. These are accomplished as follows -

1. To use computational fluid dynamics based methods to study the movement and deposition of particulate aerosols in a monolith channel of a DPF (fully Eulerian single phase simulations assuming inert particulates).

   - Solve for Brownian diffusion as a passive scalar transported in a fluid field given by the in-compressible Navier-Stokes equations.
   - Identify if there are any deficiencies with such a simplified treatment.
   - Propose alternate methods that can complement or supplement this treatment.

2. To develop a more rigorous numerical method that can handle (and overcome the

deficiencies of the fully Eulerian treatment) the transport and deposition of realistic particulate aerosols in monolith channels.

- Extend the ideas from traditional Langevin based Lagrangian treatment of Brownian nano-particles (such as the Ounis and Ahmadi model [64]) towards transport and deposition of particulate aerosols in a monolith channel.

- Utilize well established multiphase DNS frameworks (for example the Immersed boundary (IB) method), that can simultaneously handle both the particulate phase and the surrounding fluid phase, to study these dispersed particulate aerosols.

- Demonstrate the capability of this novel method: Evaluate the diffusion dynamics (mean square displacements, velocity auto-correlation functions and diffusivities) of an ideal spherical soot particle.

- Extend the applicability of the method to describe the particle dynamics of a real fractal shaped soot particle.

1.4 Document structure

This thesis is organized in a similar manner as the aims that are defined in the previous section (Section 1.3). Consequently, the second chapter discusses the fully Eulerian single phase simulations of the transport of particulate aerosols in a monolith channel. A brief overview of the numerical method (including the governing equations), the numerical set-up and the critical results from this analysis are provided in this chapter. In the third chapter we briefly describe the traditional Langevin equation based Lagrangian treatment of particulate aerosols. The results presented in this chapter would be used as the benchmark to evaluate the performance of the novel multiphase DNS method that has been proposed in this work. Subsequently, the next (fourth) chapter describes the more numerically rigorous multiphase DNS framework including a detailed account of the chosen technique (i.e. the Immersed boundary method coupled to a solver for evaluating the Langevin dynamics) along with the employed numerical setup and some critical findings from this assessment. This chapter also describes the extension of this IB based multiphase DNS method to study the diffusion dynamics of a real soot particle (with a fractal shape). The last chapter presents some preliminary conclusions from this work and highlights further scope of this research. The relevant papers are appended in the end of this thesis.

Chapter 2
Eulerian treatment of particulate aerosols

Traditionally the (diffusion) dynamics of nanoscale particles in a viscous fluid are studied in a Lagrangian framework (using a Langevin description), as will be explained later [43, 10, 64, 65]. Such dynamics are best represented by a diffusivity (particularly as the probability distribution function for particle displacements is Gaussian at all times), which is a measure of the mobility or rate of the diffusion process. Chandrasekhar [10] discussed an analogy between random flight (i.e. Brownian motion) and diffusion and showed that the motion of a large number of individual particles subjected to random flights without mutual interference can be described as a diffusion process. Hence, as a first approximation (and thereby minimizing the computational cost) a fully Eulerian model derived on the assumption of inertialess inert particles is employed to estimate the particle dynamics (transport and deposition) of a large number of small particles (with a fixed Brownian diffusivity) in the substrate channel. The details about this treatment are provided in this chapter. A brief overview of the governing equations as well as some of the inherent assumptions and limitations of this method are described in the early sections. This is followed by a brief account of the numerical set-up and an overview of the critical results from this assessment.

2.1   Governing equations

The Brownian deposition of particulate aerosols in a fully Eulerian single phase framework (on the assumption of inertialess particles i.e. in the limit St $\rightarrow$ 0), can be studied as a passive scalar (species) transported (by convection and diffusion) in a fluid field given by the in-compressible Navier-Stokes equations -

$$\frac{\partial u_j}{\partial x_j} = 0$$
$$\frac{\partial (\rho u_i)}{\partial t} + \rho u_j \frac{\partial u_i}{\partial x_j} = -\frac{\partial p}{\partial x_i} + \frac{\partial \sigma_{ij}}{\partial x_j} \tag{2.1}$$

where σ_{ij} is the viscous stress tensor

$$\sigma_{ij} = \mu \left(2S_{ij} - \frac{2}{3}S_{mm}\delta_{ij} \right), \tag{2.2}$$

S_{ij} is the strain rate tensor

$$S_{ij} = \frac{1}{2}\left(\frac{\partial u_i}{\partial x_j} + \frac{\partial u_j}{\partial x_i} \right) \tag{2.3}$$

The passive scalar transport (convection-diffusion) equation that is solved along with Eq. 2.1 is given as:

$$\frac{\partial \epsilon_k}{\partial t} + u_j \frac{\partial \epsilon_k}{\partial x_j} = D_k \frac{\partial^2 \epsilon_k}{\partial^2 x_j},$$

(2.4)

with D_k given as -

$$D_k = \frac{k_B T C_c}{3\pi \mu d_{p,k}},$$

(2.5)

here, ϵ_k is the dimensionless concentration (i.e. *mass concentration/mass fraction*) of a passive scalar representing an ensemble of particles of size $d_{p,k}$ with Brownian diffusivity D_k as given by Einstein [19]. Note that, this approach requires one additional transport equation (c.f. Eq. 2.4) for every particle size considered, but imposes no additional need for averaging or any other time step limitations.

The simplifications employed in the Eulerian model, i.e. assumption of ideal inertia-less inert particles in the limit St $\rightarrow$ 0, would mean that there are some inherent limitations with it. These are listed below -

- The system is one-way coupled i.e. the fluid is not affected by the concentration fields.

- The Schmidt numbers are large, i.e. $Sc = \frac{\mu}{\rho D_k} >> 1$, meaning that a finer mesh is needed to resolve the steep concentration gradients close to the particle surface.

- The Eulerian model requires elaborate extensions to incorporate history effects to the particle motion (when they are relevant).

In spite of these limitations, the Eulerian framework is still a powerful tool that can be used to assess the deposition of inert particulates.

2.2 Numerical setup

The simulations were setup based on experiment trials that were conducted on the exhaust from a Volvo D5 diesel engine with five cylinders and a displacement volume of 2.4 L that used low-sulphur diesel (see Table 2.1). The exhaust gases are passed through a generic exhaust after treatment rig: EATS (emission after treatment system) that creates a systematic variation of the emissions with respect to residence time, temperature and gas phase compositions by using different set-ups e.g. adding air (upstream dilution) or different types of substrates (monolithic catalysts). Two inactive cordierite monoliths (5.66 inches by 6 inches) from Corning Inc. were studied (in the experiments): one bare substrate and one coated with 6% w/w alumina. The uncoated monolith had square channels with a (hydraulic) diameter of 1.12 mm while the coated monolith was treated as having circular channels with a diameter of 1.09 mm. A fast particle analyser (DMS500) is used in the EATS set-up to measure the PSD changes across the monolith (this is reported as capture efficiency or deposition efficiency in the Fig. 2.2). A more detailed account of these experimental trials are available in [74].
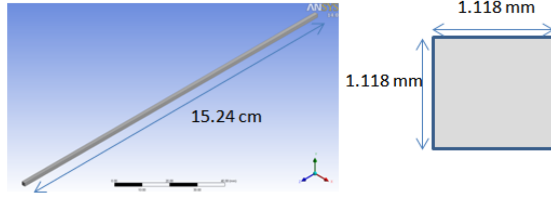
Figure 2.1: *3D Square monolith channel (left) and inlet cross-section of channel (right).*
.

Consequently, a square monolith channel of dimensions *1.118 mm by 1.118 mm* and a length of *15.24 cm* has been modelled (based on standard dimensions for the monolith channel from experiments). A schematic of the geometry employed in these simulations is shown in Fig. 2.1. The domain boundary conditions are: a constant velocity over the inlet, a constant (atmospheric) pressure over the outlet, and no-slip at all walls. A constant velocity over the inlet is deemed a realistic inlet boundary condition since the dimensions of the channels are small in relation to the velocity gradients of the mean flow upstream to the catalyst. Additionally,the equation system presented earlier (c.f. Eqs 2.1, 2.4 and 2.2) is solved with the boundary conditions that $x_k = 0$ on any wall where the PM may deposit, and $x_k = x_k^*$ (i.e. an arbitrary set value) at the domain inlet. The deposition efficiency for nanoparticles of size $d_{p,k}$ is obtained by relating the mass-averaged value of x_k on the domain outlet to x_k^*. The equation system is discretized using the QUICK scheme [44] for the convection terms and a second-order accurate central differencing scheme for the diffusion terms. The temporal discretization is second-order implicit. These system of equations were solved in the commercial computational fluid dynamics (CFD) package `Ansys FLUENT`.

Table 2.1: Case data for the experimental tests with diesel soot nanoparticles reported in Figs. 2.2 and 2.3. *Addition of air* indicates whether air has been added to further dilute the exhaust gas flow after the engine but before the catalyst substrate, the main point of which is to change the gas-phase concentrations of background HCs. The two substrates represent a bare (Cordierite without a wash coat) and a coated substrate (Cordierite with a 6 % w/w alumina wash coat).

Case	Substrate	Temperature in substrate $(\deg C)$	Reynolds number	Retention time in channel (s)	Addition of air
A1	Cordierite	222	2.7	1.74	No
A2	Cordierite	263	8.1	0.5	No
A3	Cordierite	157	11	0.55	No
B1	Alumina	164	8.3	0.68	Yes
B2	Alumina	163	2.4	2.36	Yes
B3	Alumina	160	2.3	2.48	Yes
B4	Alumina	154	2.0	2.95	No

2.3 Results: Diffusion in open substrates

The numerical simulations were set-up based on the detailed experimental campaign on an EATS rig for diesel engine generated PM aerosols (c.f. Table 2.1). Mesh independence was first established by simulating laminar flow through the channel. The mass weighted average of the dimensionless outlet concentration (ϵ_k) from 5 different fluid meshes are compared to determine mesh independence . Based on this, a mesh with around 927000 cells is chosen for all the simulations done with this framework. Next, the cases in Table 2.1 were simulated with an arbitrarily chosen inlet mass fraction of 0.01 (for the passively transported inert particles). The deposition or capture efficiency (CE) from the simulations are estimated using the changes in mass weighted average of the mass fraction of the passive species at the inlet and outlet of the channel as follows -

$$CE = \frac{mass\ fract_{in} - mass\ fract_{out}}{mass\ fract_{in}} \tag{2.6}$$

2.3.1 Diffusion of PM: assuming inert particulates

The deposition efficiency (Eq. 2.6) of the engine-generated diesel particulate matter in a monolith substrate (both coated and uncoated) could not be well described by the Eulerian model as illustrated in Fig. 2.2. More specifically, the experimental deposition efficiency is significantly higher than the theoretical prediction. However, the relative qualitative trends in the numerical predictions are consistent with the experimental results, in that the most pronounced dependency of the deposition efficiency seems to be the retention time in the substrate – with longer retention times producing higher deposition efficiencies. It can also be seen that the agreement is relatively acceptable for particles larger than 100 nm (disagreement increases with decreasing the particle size).Effects such as inertial impaction in the front of the substrate and thermophoretic deposition (i.e. PM migration in the direction of decreasing temperature) cannot be responsible for such a huge difference. Moreover, there are no obvious explanations for the disagreement between the experimental and the numerical results, except for the fundamental assumption that the particles were inert.

Hence, to verify if the Eulerian model can indeed capture the deposition of inert PM aerosols in an open-substrate, the EATS experiments were rerun with cubic-shaped NaCl crystallites that closely resemble inert spheres (an idea proposed in Tumolva et al. [82]). The EATS rig is used to study the deposition of these solid nanoparticles that were generated by atomizing a salt (NaCl) solution followed by drying the droplets in a heated tube. The deposition (or capture) efficiency from this experimental study is compared with the corresponding simulation (now the assumption about inert particles is appropriate). The critical result from this assessment is presented in Fig 2.3. It can be seen quite clearly that for truly inert particles, the Eulerian model does successfully predict the deposition of ultra-fine PM aerosols in an open substrate. This observation further lends credibility to the assumption that a model for reactive PM (including particle transformations) is indeed the missing link in the study of realistic soot nano-particle deposition. Some more

detailed results from this evaluation with inert cubic shaped NaCl crystallites are available in [73, 37].
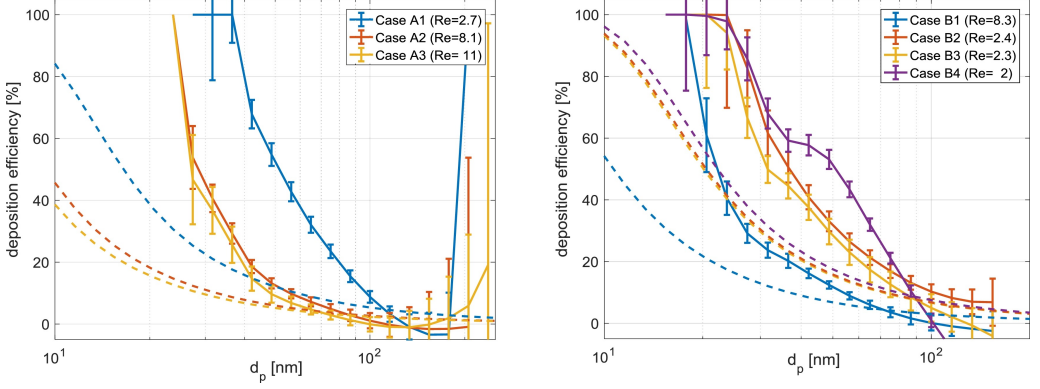
Figure 2.2: *Deposition efficiency of engine-generated nanoparticles in a bare cordierite substrate (left) and an alumina-coated substrate (right). The solid lines are experimental values and the dashed lines are simulations. The error bars represent confidence intervals.*
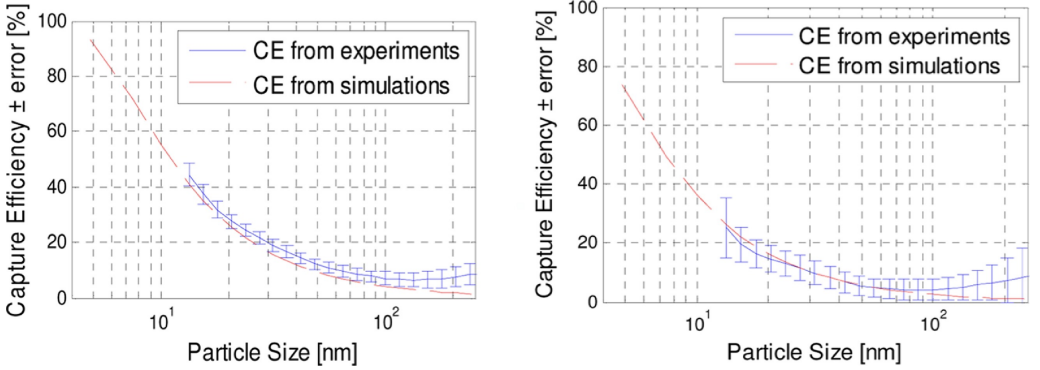
Figure 2.3: *Deposition efficiency of NaCl nanoparticles in a bare cordierite substrate at $Re = 7.8$(left) and $Re = 24$ (right) at $150 \deg C$. The error bars represent confidence intervals. Note the similarities between experiments and simulations.*

2.3.2   Diffusion of PM: assuming reactive particulates

Further, to accommodate a realistic description of PM deposition, a simple conceptual model that assumes that the PM aerosol is a mixture of three different types of particles: truly inert particles, semi-volatile particles and completely volatile particles, has been used to establish the need for reactive particulates. A detailed account of this conceptual model and its inception is available in [73] and in the appended Paper A. The experimental measurements from the EATS rig (ref Table 2.1) are used to ascribe the distribution

of the three conceptual particle types, including an estimate on the amount of volatiles semi-volatiles (in terms of mass and molar fractions) [74]. Eight parameters ($A1$, $A2$, $B1$, $B2$, K, Q, $M1$ and $M2$) are fitted to the experimental data for two sigmoidal functions HC_{part} (which is the size resolved number fraction of pure volatile particles) and HC_{frac} (which is the size resolved mass fraction of volatiles of the remaining particle i.e. when HC_{part} is subtracted (see Eqs. 2.7 and 2.8 below).

$$HC_{frac}(d_p) = A_1 + \frac{K - A_1}{[1 + Qexp\{-B_1(log_{10}d_p - M_1)\}]^{1/Q}}, \qquad (2.7)$$

$$HC_{part}(d_p) = A_2 - \frac{A_2}{[1 + Qexp\{-B_2(log_{10}d_p - M_2)\}]^{1/Q}}. \qquad (2.8)$$

This conceptual model is coupled with a model for decrease in particle size (to account for realistic PM transformations) to estimate the PM deposition in the monolith channel. The decrease in particle size is best described by the hydrocarbon evaporation model of Giechaskiel and Drossinos [24] (as given below) -

$$\frac{\mathrm{d}d_p}{\mathrm{d}t} = \frac{2M\alpha_c\,(p_\infty - p_d)}{\rho_p N_A \sqrt{2\pi m k_B T}}, \qquad (2.9)$$

where M is the molecular mass of the hydrocarbon, α_c is a condensation coefficient (obtained from [24]), p is the partial pressure of the hydrocarbon in the bulk (∞) and on the surface of the particle (d), N_A is the Avogadro's number and m is the mass of one hydrocarbon (HC's) molecule.

As a quick first estimate, the deposition of PM (including realistic transformations) was assessed using the tanks-in-series (TIS) framework. This method evaluates PM transport by studying the evolution of the concentration distribution through a series of N fully mixed tanks. This is given by the molar/mass balance across each individual tank as follows -

$$V\frac{\mathrm{d}c_{k,n}}{\mathrm{d}t} = q\,(c_{k,n-1} - c_{k,n}) - \frac{D_k Sh A c_{k,n}}{d_h}, \qquad (2.10)$$

where V is the volume of the tank, $c_{k,n}$ is the concentration of particles of size and type $d_{p,k}$ (which varies according to Eq. 2.9) in tank n, q is the volumetric flow rate of gas, A is the total wall surface area available in the tank, $Sh = \frac{k_c d_h}{D_k}$ is the Sherwood number for a monolith channel with hydraulic diameter d_h and convective mass transfer coefficient k_c. The deposition efficiency for nano-particles with initial size $d_{p,0}$ and Brownian diffusivity $D_k(d_p)$ is obtained by relating $c_{k,0}$ to c_{k,n_t}, where n_t is the last tank.

The TIS framework is used to fit the experimental data [73] with a simple numerical estimation of PM deposition. After the fitting procedure is finished, the predicted deposition efficiency is compared to the experimentally obtained one (see Fig. 2.4).As shown in the right panel of Fig. 2.4, using the TIS framework with the conceptual model for particle transformations improves the agreement between experimental observations

and numerical results in terms of particle deposition efficiencies. Such a close agreement is an expected result, given the successful indirect validation of the hypothesis that the PM deposition cannot be fully accounted for by assuming inert particles (c.f. Figs. 2.2 and 2.3). Subsequently, we have also validated the TIS implementation of the conceptual models against its implementation into a comprehensive Eulerian-Lagrangian framework [73]. Thus, there is a need to account for particulates in the exhaust gas from vehicular exhausts as reactive.
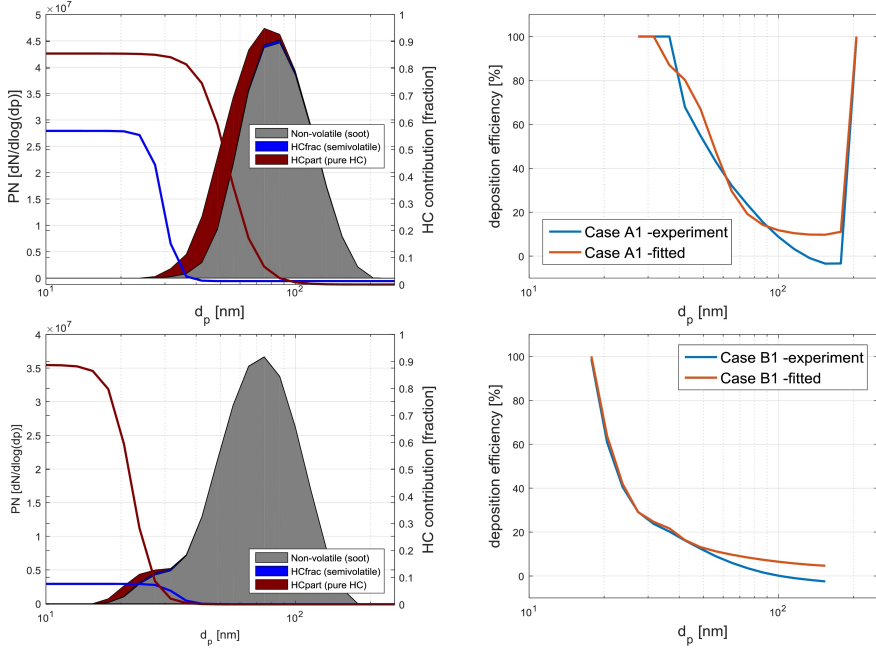
Figure 2.4: *Particle size distribution (left) and deposition efficiency (right) of engine-generated diesel particulate matter in a bare cordierite substrate, Re = 2.7 (top) and in an alumina-coated substrate, Re = 8.3 (bottom).*

Hence, a clear deficiency of a purely Eulerian treatment derived on the assumption of inertialess inert particles has been identified. There is a clear need for a more detailed account of the reactive nature of the PM (including its transformations) and its transport in traditional exhaust after treatment devices (such as the monolith channels in a DPF). This deficiency would be addressed by introducing and utilizing frameworks that can resolve particle dynamics more thoroughly (in the remaining parts of this thesis). Consequently, we will discuss a purely Lagrangian description of the system and a more rigorous multiphase treatment (that can resolve the complex particle-fluid coupling encountered in these applications).

Chapter 3
Lagrangian treatment of particulate aerosols

The diffusion dynamics of particulate aerosols which are dilute can be more accurately described using a Lagrangian treatment. In this method, the particle equation of motion (Newton's second law i.e. $m\frac{dv}{dt} = \Sigma Forces$) is solved for each particle by considering them as point masses (i.e particle has negligible volume but a finite mass or inertia). This approach is more apt for studying the deposition of reactive particulates, as any morphological change in them (such as decrease in the diameter as given by the by the hydrocarbon evaporation model of Giechaskiel and Drossinos [24]) can be easily incorporated in the governing equations. In fact, the Langevin equation which is widely regarded as the governing equation for the Brownian dynamics of micro and nanoscale particles (in a fluid) can be solved in a Lagrangian frame of reference [43, 10, 64, 65]. In this chapter, we discuss the well established Langevin treatment. We further describe some simple cases for the diffusion of an ideal inert spherical particle in an unbounded domain (channel). The particle dynamics are evaluated in terms of mean squared displacements, velocity auto-correlation functions and diffusivities and results from this assessment are reported.

Note that we have not extended this treatment towards reactive particulates, particularly at this stage of the work. This is because the preliminary aim is to establish a rigorous numerical tool for describing PM deposition in exhaust after treatment devices (such as the monolith channels in a DPF), and a purely Lagrangian treatment would still be missing a very essential portion of the particle-fluid coupling (i.e. we do not resolve the fluid phase around the particle). Moreover, when the particulate flows are dense, as is the case in the monolith channels of a DPF, the particle-fluid coupling is more pronounced and the Lagrangian framework breaks down due to the violation of the point-particle assumption (i.e. the particle volume is not negligent any more). Nevertheless, the results from such a Lagrangian treatment serve as benchmarks which can be used to validate the performance of the more rigorous multiphase frameworks (which are described in this thesis).

3.1   Governing equations: The Langevin treatment

In this thesis, we are concerned with the transport of particulates in the size range 80 nm to 1000 μm, which would mean that particle sizes are very close to the mean free path (molecular length scales) of the surrounding fluid. Hence, non-equilibrium behaviour must be exhibited, meaning that the particulate phase would interact with the constitutive molecules or atoms of the surrounding fluid. This results in two primary effects. Firstly the regular collisions act as a random driving force on the particle maintaining an incessant irregular motion and secondly, they give rise to a frictional force (or drag) for a forced motion. The superposition of these two opposing effects gives rise to a meandering motion commonly referred to as *Brownian motion*. This fundamental theory of *Brownian*

diffusion was established by Einstein [19] and Smoluchowski [77] for the diffusion of micro-scale particles in a viscous fluid and was further extended by Langevin [43]. It is this random motion of particles that drives the deposition/diffusion process in exhaust gas after-treatment devices (as explained earlier c.f. Section 1.2). Note that we refer to such aerosols as rarefied aerosols, meaning that the particle length scales are similar to the molecular length scales of the surrounding fluid.

3.1.1 Langevin equation

The fundamental theory of Einstein and Smoluchowski is restricted to time scales at which the decay time of the velocity of the Brownian particle is negligible (i.e much larger than the particle response time). Hence, a more complete description of the Brownian motion of a *free particle* was proposed by Langevin [43, 10], as shown in Eq. 3.1 -

$$\frac{\mathrm{d}\mathbf{u_p}}{\mathrm{d}t} = -\gamma\mathbf{u_p} + S(t),\tag{3.1}$$

where, $\mathbf{u_p}$ denotes the velocity of the particle, while γ and $S(t)$ denote the systematic (a dynamical friction) and fluctuating part of the Brownian description of particle motion. It should be noted that both these parts are related as they are a result of the same underlying phenomenon, i.e. random collisions with the surrounding molecules. The frictional term γ is generally described by the steady Stokes drag [78] for fluids at rest. The fluctuating component $S(t)$ is assumed to be independent of the velocity u_p and further fluctuate very rapidly in comparison with variations in the velocity. Uhlenbeck [83] further showed that Eq. 3.1 is constrained by certain restrictions on the fluctuating component $S(t)$, i.e. it follows a Gaussian white noise process. Additionally, $\langle S(t)\rangle = 0$, where $\langle ...\rangle$ denotes an ensemble average in thermal equilibrium.

Hence, the Langevin equation (3.1) is the momentum equation for the particle with a random forcing for the non-equilibrium behaviour and with a friction force linear in instantaneous velocity. Solving this stochastic differential equation (SDE) provides a detailed insight into the diffusive behaviour of the nanoscale particulates as well as furnishes additional details including the velocity auto-correlation function (the correlation of the present particle velocity with the velocity at other times). The Langevin equation is valid provided the following two assumptions are met -

1. The random forcing appears as a white noise at a scale lesser than the particle response time τ_p (i.e the time scale of a particle slowing down owing to friction from the fluid after an initial impulse)

2. The hydrodynamic coupling between the particle and the fluid (i.e. the fluid friction) is given by the steady state Stokes drag [78] (the friction force is linear in the instantaneous velocity)

The white-noise assumption is satisfied when the particles are much larger than the surrounding fluid molecules without being much less dense [30]. The validity of the steady state drag has been a source of debate for several applications of the Langevin treatment,

especially when the particle-fluid density ratios are lower (i.e unsteady effects such as basset history and added mass forces begin to play a role) [67, 3, 30]. However, for typical particulate aerosols generated by combustion of vehicular fuels, the particle-fluid density ratios are significantly higher, meaning that the hydrodynamic coupling can be given by steady hydrodynamic forces and hence the Langevin equation is perfectly suited to study these systems. There is however another complication and this concerns the continuum form of the Stokes steady state drag. This is addressed below.

3.1.2   Is the continuum formulation for the steady drag still valid?

The Langevin equation constitutes of a force balance between the hydrodynamic drag and the Brownian fluctuations. However, under the typical conditions encountered in exhaust after treatment systems such as monolith channels of a DPF (i.e. deposition of PM in a size range 1 nm to 1 μm) these particulates do not experience the surrounding fluid as a continuum. This is because the continuum assumption begins to break down when the characteristic dimensions of the flow are comparable to the mean free path of the constitutive molecules (in this case air has a mean free path of $\approx$ 67 nm at 20 degC and atmospheric pressure). Under such conditions, the fluid can no longer be regarded as being in thermodynamic equilibrium and a variety of *non-continuum or rarefaction effects* are likely to be exhibited [6]. Consequently, the no-slip boundary condition, traditionally employed at the particle surface, is no longer applicable and a sub-layer (the Knudsen layer) of the order of one mean free path starts to affect the fluid interaction between the bulk flow and the particle.
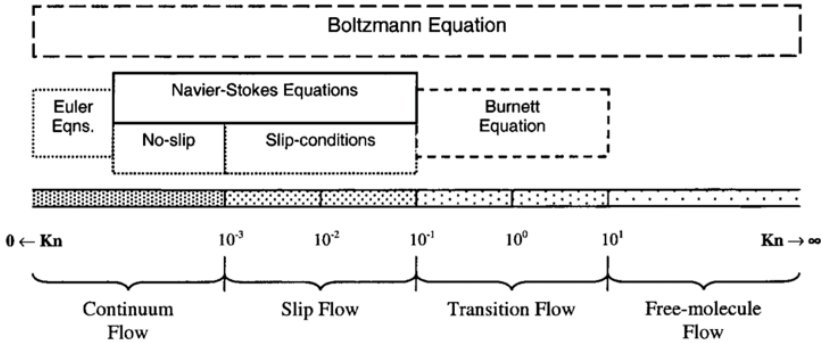
Figure 3.1: *Flow regimes classified based on the Knudsen number (figure adapted from Roy et.al [70]).*

The applicability of the continuum assumption can be determined based on the dimensionless Knudsen number ($Kn = \frac{2\lambda}{d_p}$), defined as the ratio of the mean free path (λ) of the surrounding fluid to the characteristic length scale of the particle (d_p), as shown in Fig. 3.1. Systems which are strongly rarefied or at the *limit of free molecular flow* are characterized by a Kn greater than unity while those which are at the *continuum flow limit* are characterized by a Kn much lower than unity. As Kn increases, the rarefaction

effects become more pronounced and eventually the continuum assumption breaks down. Hence, the particle-fluid interaction has to be resolved by solving the Boltzmann equation instead. Nevertheless, conventional continuum descriptions of the forces can be extended to describe the *transitional and slip flow* regimes by imposing appropriate slip and temperature jump boundary conditions on the surface [6].

Early attempts at understanding such rarefied flow regimes at low densities began with Maxwell [53], when he derived a slip boundary condition for a dilute gas using kinetic theory. This idea was extended by Cunningham [12], who derived an empirical first-order slip velocity correction factor from hydrodynamic theory for small Kn. Further, Millikan [54] confirmed (with experimental evidence) that the drag reduction (due to hindered momentum transfer between the particle and fluid) at higher Kn can be deduced using the Cunningham correction (C_c), making this an invaluable correlation to study the rarefaction effects even up to the transition regime (c.f. Fig. 3.1).This is proposed as a function of Kn as shown below.

$$C_c(Kn) = 1 + AKn, \tag{3.2}$$

where A is further a function of Kn that is determined based on empirical data. The Cunningham correction produces results that are in excellent agreement with the available experimental data as shown by Alan and Raabe [4]. Mosfegh et.al.[57] summarize the Cunningham-based slip correction factors (and corresponding A values) that have been proposed and commonly used by researchers (based on extensive experimental trials), for air with mean free path of 67.3 nm at 101.3 kPa and $23°C$. Among these, the most commonly used relation was the one proposed by Davis [13] and is given as -

$$C_c = 1 + Kn \left(1.257 + e^{\frac{-1.1}{Kn}} \right). \tag{3.3}$$

Other higher-order slip conditions have also been postulated in literature, however these formulations are not trivial and highly geometry dependent [11]. A simple, yet formally second-order general slip condition was proposed by Karniadakis et al.[38]. However, there is not yet a consensus in open literature neither on the best choice for a higher-order slip formulation, nor on their advantages in complex geometries. Further, most higher order slip correction methods already fail at very low Knudsen numbers ($Kn < 0.1$) [9] for solid-liquid systems. An added complexity in these aerosol systems is that the dimensionless Knudsen number (Kn) is in the transition regime ($10^{-1} < Kn < 10^1$) meaning that extending the continuum description is challenging. Hence, we have to resort to the more empirically based Cunningham correction in this thesis, and this is described below.

3.1.3 Extended Langevin approach: Inclusion of the Cunningham correction

In order to be applicable for gas-solid rarefied flows, the ordinary Langevin equation (Eq. 3.1) is extended to include the Cunnigham correction C_c (first order slip correction

for rarefaction) for a particle with mass m_p and velocity $\mathbf{u_p}$ as developed by Ounis and Ahmadi [64, 65] -

$$m_p \frac{d\mathbf{u_p}}{dt} = -\gamma_C \mathbf{u_p} + \mathbf{F_{unsteady}} + \mathbf{F_{Brownian}}(\mathbf{t}), \qquad (3.4)$$

where γ_C is the Stokes friction factor (Eq. 3.5) including the Cunningham correction (C_c). $\mathbf{F_{unsteady}}$ and $\mathbf{F_{Brownian}}(\mathbf{t})$ are the unsteady and stochastic effects experienced by a Brownian particle. γ_C is defined for a fluid with dynamic viscosity μ_f as -

$$\gamma_C = \frac{3\pi \mu_f d_p}{C_c}, \qquad (3.5)$$

where the particle time scale is given as

$$\tau_p = \frac{1}{\gamma_C} \qquad (3.6)$$

$\mathbf{F_{Brownian}}(\mathbf{t})$ is modelled as a Gaussian white noise process with spectral intensity S_{ij} given as -

$$S_{ij}^n = S_0 \delta_{ij}, \qquad (3.7)$$

where S_0 is a function of the Brownian diffusivity $D = \frac{k_B T}{\gamma_C}$ of the particle -

$$S_0 = \frac{2D\gamma_C^2}{\pi}. \qquad (3.8)$$

Thus, $\mathbf{F_{Brownian}}(\mathbf{t})$ can be written as -

$$\mathbf{F_{Brownian}}(\mathbf{t}) = m_p G \sqrt{\frac{\pi S_0}{\Delta t}}, \qquad (3.9)$$

where, G is a normally distributed independent random number and Δt is the time step length at which the Brownian force is active (note that this is not necessarily the time step used in the integration of the particle equation of motion, as will be explained later). Ounis and Ahmadi [65] and Maxey and Riley [52] showed that the unsteady drag effects, i.e. $\mathbf{F_{unsteady}}$ (added mass, the Basset history term and the Faxen corrections) are negligible for sub-micron aerosol particles, hence these can be omitted.

The solution to Eq. 3.4, sans the unsteady effects, will reproduce the following analytical diffusive behaviour as postulated by Einstein [19]. For a number of particles diffusing over time, the root-mean-square displacement (MSD) distance in one dimension (MSD_x) should equal the standard deviation σ_{1D} of the Gaussian probability density function, i.e. -

$$MSD_x = [\frac{1}{N} \sum_{n=1}^{N} (x(t+dt) - x(t))^2]^{\frac{1}{2}} = \sigma_{1D} \equiv \sqrt{2D_C \Delta t}, \qquad (3.10)$$

18

It should however be stressed that the solution (or solution process) to Eq. 3.4, a stochastic differential equation (SDE), is not synonymous with the commonly encountered ordinary differential equations (ODE). The integration of these SDE's are constrained by certain properties of the stochastic time integral as first defined by Itô [33]. To understand these constraints let us split the integral time interval into a number of small time steps, which are then summed to give the final solution. This limit result is not independent of the choice of the intermediate time, which is used while splitting the solution into smaller time steps, as one would expect from classical Riemann integration laws [7]. This is because the solution would change depending on the time point at which the integration is started, as these are random time evolving systems (the trajectories have infinite variation). Hence, it is very important to decide on the sense or form of the integral which should be solved. The Itô sense, which has a clear probabilistic interpretation and is most often used to describe Brownian processes, assumes that the integral is solved from the beginning of the time interval. This interpretation is most convenient for numerical simulations because the increment of the stochastic process is uncorrelated with the variables at the same time. This would mean that, forward stepping explicit schemes are preferred while solving SDE's in an Itô sense . More generally, higher order schemes (such as higher order Runge-Kutta schemes) can introduce spurious drifts in the solution and should be avoided [55].

It should be noted that a purely Lagrangian method such as the one described here, has a few inherent limitations -

- The flow around the particles is not resolved (only fluid-particle coupling is modelled through various forces such as drag, added mass etc.).

- The models proposed for the various forces are based on the point-particle assumption and hence the Lagrangian treatment works best for unbounded flows where $d_p \ll h$ (channel dimension)

- In order to generate the relevant diffusion dynamics, the particle statistics have to be ensemble averaged over several trajectories, meaning that this approach can get very cumbersome computationally.

- This treatment cannot handle two-way (both particle and fluid affect each other) or four-way coupled (particle-fluid and particle-particle interactions) systems as once again the models for the various forces have to be altered to include these effects.

Hence, a purely Lagrangian treatment is ill-suited for studying the transport and deposition of PM in the monolith channels of a DPF. Particularly as both the channel and pore dimensions can shrink due to the build-up of deposited PM (i.e. the particle and the pore dimensions are not too dissimilar, violating the point-particle assumption). Nevertheless, it can still be used to generate relevant benchmarks for unbounded diffusion of particles, which can be used to evaluate the performance of more rigorous multiphase frameworks (as will be done in this thesis).

3.2 Numerical setup

The Ounis and Ahmadi [64, 65] treatment is assessed in a Lagrangian framework. The particle equation of motion is integrated using a forward Euler explicit time marching scheme (to solve the extended Langevin equation Eq. 3.4) including the corrected Stokes drag (Eq. 3.5) as the only hydrodynamic coupling between particle and rarefied gas (the fluid flow is not solved for). This would mean that this is a one-way coupled gas-solid system which is stochastically forced by the relevant model for Brownian motion (Eq. 3.9). The time step chosen for the integration of the SDE is based on the particle response time $\tau_p/10$. The stochastic forcing is applied at every $\tau_p/10^{th}$ response time (i.e. the Brownian motion is resolved over 20 time-steps). This was deemed necessary so as to have a good resolution of the Brownian motion. This assessment was done using a solver written in a `Python` environment.

It should be noted that in our assessments we include the Cunningham correction within the particle density ρ_p as opposed to directly correcting the Stokes drag. Hence, we simulate a heavier particle i.e. the same drag reduction is reproduced by having a scaled particle density ($\rho_p C_c$). Correspondingly, the Boltzmann constant (k_B) is scaled with the Cunningham correction as well to have the correct Brownian diffusivity D (as in Eq. 3.5). In a nut shell, by doing this we reproduce the exact behaviour as that of the normal Ounis and Ahmadi treatment (3.4). Consequently, the particle dynamics is calculated using the uncorrected Stokes drag.

3.3 Results: Langevin treatment in an unbounded domain

In this section we study unbounded Brownian diffusion at sufficiently high particle-fluid density ratios in Stokes flow as given in Table 3.1. The results from this assessment are used to establish the benchmarks that would be used to evaluate the more rigorous multiphase frameworks used in this thesis. Further, these simulations would also serve as the basis for deciding on the simulation duration along with other statistically relevant criteria that are needed to describe the particle diffusion dynamics. Note that the random seeds that have been used to initiate the stochastic process in these simulations would be used in the corresponding multiphase DNS treatments as well. This is done to ensure that we compare similar stochastic processes while benchmarking the frameworks.

3.3.1 Langevin diffusion of a 400 nm speherical particle

The diffusion dynamics are typically quantified via the mean squared displacement (Eq. 3.10). The displacement of the particle can be defined for different time intervals (or time lags or lag times) between positions *(x, y, z)* with the number of possibilities limited to the duration t of the simulation. In this work, we evaluate a single particle trajectory over very long periods of time. This in-turn represents multiple particle trajectories ensemble averaged over much shorter duration. Some typical results from particle diffusion dynamics

Case	Particle/Fluid density ratio
DBP1	2000
DBP2	1000
DBP3	500
DBP4	100

based on the conditions in Table 3.1 are shown in Fig. 3.2. Particle trajectories and the *MSD* of the particle are depicted in the panels Fig. 3.2 a and b respectively. The *MSD* is non-dimensionalized by the diffusional length scale ($MSD^* = \frac{MSD}{\sqrt{D_c \tau_p}}$). Such a non-dimensionalization of the results would compensate for the density dependence of diffusivity. This would mean that, if Stokes drag is the only hydrodynamic coupling, there should be no differences in the MSD^* across the simulations with different particle-fluid density ratios (as seen in Fig. 3.2b).

(a)   (b)
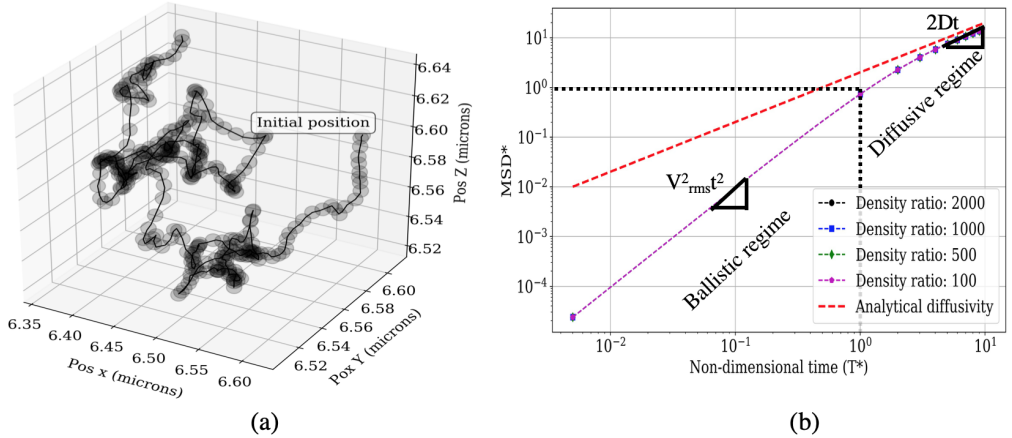
Figure 3.2: *Particle diffusion dynamics : a) Brownian trajectory of a 400 nm diameter particle (with density 1000 kg/m³) and b) Non-dimensional MSD after a lag time of 10 response time units across different density ratios after 150 response times (the slopes indicate the ballistic and diffusive regimes). The red dashed lines (-- --) represent the Einsteins analytical diffusivity (Eq. 3.10).*

Further, this figure also depicts a very important property of Brownian diffusion, i.e. transition from a ballistic to a diffusive regime. The stochastic description of the interactions of the particle with the surrounding fluid breakdown at the shortest timescales, where the particle's inertia is dominant. In this inertia-dominated regime, termed as ballistic, the particle's motion is highly correlated and therefore a definition of velocity is plausible (i.e. a

root mean squared particle velocity V_{rms} given as $V_{rms} = [\frac{1}{N} \sum_{n=1}^{N} (v(t+dt) - v(t))^2]^{\frac{1}{2}})$. Correspondingly, the MSD^* approaches $(V_{rms}t)^2$ in the ballistic regime below τ_p, and reaches $2Dt$ (Einstein's result c.f. Eq. 3.10) at larger times (c.f. Fig. 3.2b). More recently, this transition between regimes has been reported in experimental work as well [31], which further confirms that the original Ounis and Ahmadi model accurately captures the Brownian diffusion of a spherical aerosol particle in Stokes flow.

3.3.2 Variation due to tail effects and random seed choice

These simple one-way coupled simulations are also used to determine the simulation duration and the lag time required to get an adequate statistical description of the diffusion process (i.e. MSD calculations). Consequently, some simulations with a time step of $\tau_p/200$ were run for a 400 nm particle (density of 1000 kg/m^3) diffusing in air. The results from this assessment are shown in Fig 3.3a. It is quite clear that as the lag time increases, the MSD estimates begin to worsen and show tail fluctuations (i.e. deviate from the analytical Einstein's diffusivity). In such cases, it is better to limit the MSD calculations to lower lag times. For instance, for a simulation that is $150\tau_p$ long, lag times up to $20\tau_p$ give the most relevant statistics. Anything higher would be prone to severe tail fluctuations. Additionally, the simulation duration also reflects on the statistics collected (c.f. Fig 3.3b). Shorter simulations would contain lesser information, and since we are only evaluating a single particle trajectory, it is always better to have the longest possible simulation (at least $150\tau_p$). Moreover, the variation in MSD across different particle trajectories (different random seeds in the stochastic forcing) is also estimated c.f. Fig. 3.4. This estimate would be used as the total variation in the stochastic process (error bars) while comparing the multiphase DNS simulations with the one-way coupled simulations. Hence, along the lines of these benchmarks, the minimum criteria that will be followed for the multiphase simulations are set as: a simulation duration of $150\tau_p$ and lag time of $10\tau_p$.

Hence in this chapter, we have discussed a Lagrangian treatment of the Langevin equation of motion for a spherical aerosol particle (in an unbounded channel) and established its validity. We have further assessed the diffusion dynamics over 150 particle response times. However, this framework cannot be used to study the PM deposition in monolith channels, particularly as the Lagrangian method fails close to the bounds of the channel (the point-particle assumption is violated). This would mean that there is a need for a more rigorous method that can handle these challenging flows (including the particle-fluid and fluid-particle coupling). Nevertheless, the results from these Lagrangian simulations will be used as a benchmark to validate the multiphase frameworks that will be described in the subsequent chapters of this thesis.
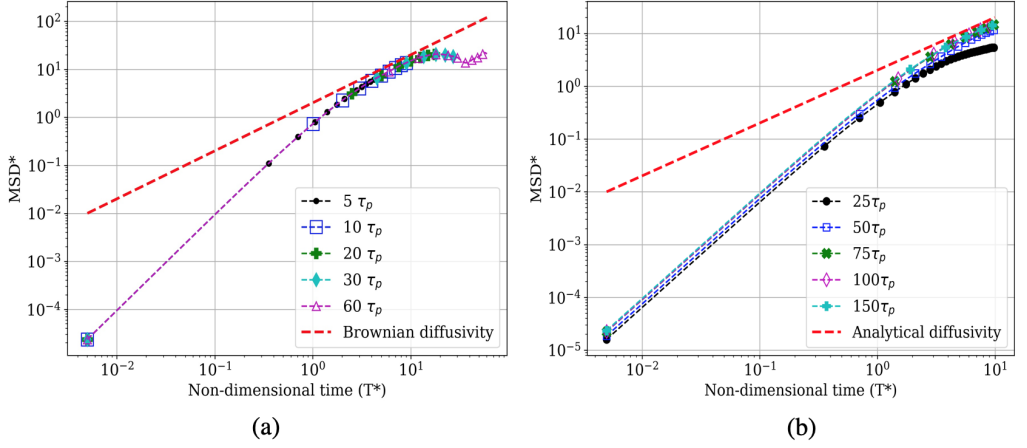
Figure 3.3: *Evaluation of tail statistics: a) Effect of lag time duration on the MSD (for a simulation duration of 150 τ_p) and b) Effect of simulation duration (in terms of τ_p) on the MSD at a time step of $\tau_p/200$ for a 400 nm particle (density of 1000 kg/m^3). The red dashed lines (- - -) represent the Einsteins analytical diffusivity (Eq. 3.10).*
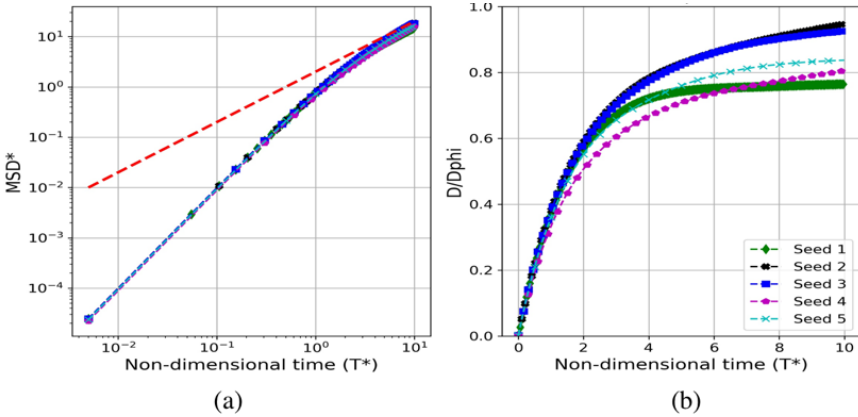
Figure 3.4: *Variation in particle diffusion dynamics across different random seeds: a) Non-dimensional MSD across different particle trajectories (different seeds) and b) Diffusivity (D_C) of the particle non-dimensionalized by Einstein's analytical diffusivity (D_{phi}) after 150 τ_p. The red dashed lines (- - -) represent the Einsteins analytical diffusivity (Eq. 3.10).*

Chapter 4
Multiphase direct numerical simulations

In the previous chapters, a single phase Eulerian (Chapter 2) and a Lagrangian method (Chapter 3) have been described in detail. It was inferred that an Eulerian treatment (derived under the assumption of inertialess inert particles) cannot accurately account for the Brownian deposition of reactive particulates in an open substrate. Further, a Lagrangian treatment does overcome some of the deficiencies of an Eulerian treatment, however it still cannot be used to study near wall and pore deposition of particulates (as the flow around the particle is only modelled and not resolved). Moreover, a deeper insight into the pore deposition phenomena would permit the designing/creation of materials/devices that would allow for more environmentally friendly and energy-efficient (clean) transportation. Hence, there is a need for a framework that can handle the complex non-equilibrium effects that arise due to the small size of the PM (the sizes are usually comparable to the mean free path of the carrier phase) in narrow geometries. This framework should simultaneously resolve the decreased momentum transfer (Cunningham slip correction) and the Brownian motion which co-exist in these non-equilibrium systems.

A straightforward way to achieve this is by performing Direct Numerical Simulations (DNS). With this technique, the Navier-Stokes equations governing the gas flow (c.f. Eq.2.1) are solved directly (using finite volume (CFD), finite element (FEM) or other numerical discretization techniques). Further, the complete flow field outside the particles is resolved accurately meaning that the particle-fluid interaction is also inherently resolved correctly. This solution of the flow is fully coupled to the particle dynamics, to ensure a two-way coupling between the phases. Such a rigorous treatment can then be used to probe phenomena in the inaccessible regions of the monolith channels (such as the pores in the wash coat), which would provide deeper insights into the PM transport and deposition phenomena.

In this chapter, we discuss some of the common multiphase DNS treatments of PM aerosols with a focus on a novel multiphase DNS method to treat the dynamics of a particulate aerosol. A brief account of the Euler-Lagrange method is also provided in this chapter. However, note that this has not been used in this study and is only presented here for the sake of completeness. The proposed novel framework is based on the immersed boundary (IB) method and to our knowledge, this is the first continuum based multiphase DNS framework that can resolve the particle dynamics of the PM aerosols. We extend the applicability of the conventional Langevin treatment of particulate aerosols (Ounis and Ahmadi method c.f. 3.4) towards this IB framework. Consequently in this chapter, we provide a detail account of the method including a brief note on Immersed boundary methods. We further demonstrate a proof-of-concept of this method, by using it to study the diffusion dynamics of a single spherical (ideal) soot particle and extend it towards a real fractal soot particle in an unbounded domain.

4.1 Euler-Lagrangian treatment: pseudo-DNS framework

In the multiphase community, the term DNS is also used for simulations where the particle motion is only modelled (i.e sometimes the flow field around the particles is not fully resolved). These pseudo-DNS methods have been used to assess deposition of particulates [73, 46], particularly if the particles are small and the flow is dilute. In most multiphase applications, it is convenient to make this assumption and further simplify the system by assuming that the particles (or clusters) do not interact with the surrounding flow (i.e. one-way coupled). Additionally, the point-particle assumption is central to the Lagrangian treatment, with the particles assumed to have negligible volume but finite mass. However, note that the flow between the particles and the particle and flow boundaries is actually resolved, and used within the particle equation of motion for e.g. Eq. 3.4 to solve for the diffusion dynamics.

The Fig. 4.1 provides an overview of such a framework. The particulate phase equations, which are usually described by the extended Langevin equation 3.4 (solved in a Lagrangian framework), are solved along with the continuum equations for the surrounding fluid (Eq. 2.1) with a suitable discretization technique (could be finite volume, finite element, finite difference etc.). The coupling between the phases is one-way (i.e. particles do not affect the fluid) through hydrodynamic drag alone. This is a reasonable assumption, given the high particle-fluid density ratios (steady effects are dominant) typically encountered in these systems as shown by Maxey and Riley [52]. This approach represents a pseudo-DNS approach in that the flow field outside the particles is not fully resolved, but instead particle motion is calculated from modelled forces.

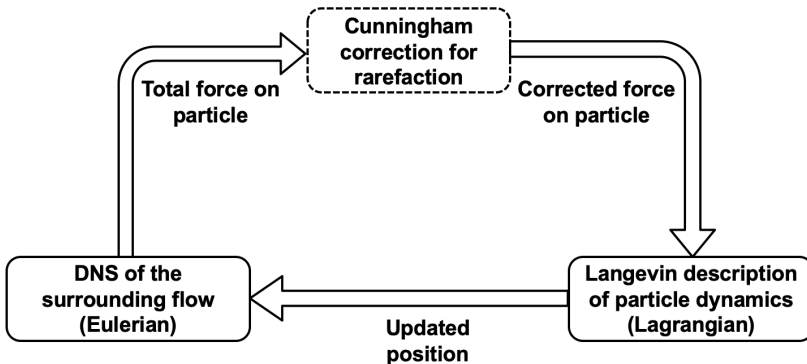Figure 4.1: *Overview of the Euler-Lagrange framework for studying PM aerosols assuming that the the total fluid force on the particle mainly includes hydrodynamic drag.*

The Eulerian-Lagrangian approach does have some inherent limitations, mainly due to the Lagrangian point-particle assumption that is central to its utilization. Most of the deficiencies of a Lagrangian treatment are applicable here as well -

- This approach is valid as long as the particulate flow is dilute (i.e. one-way coupled with the fluid) and thus cannot be used to study particle-particle interactions inside pores during pore fill-up/blocking.

- This approach breaks down when the particle is similarly sized to the flow domain (i.e. the point particle assumption is invalid), hence cannot be used to study pore diffusion.

- Similarly, the method fails close to any flow boundaries (particle-wall and particle-particle boundaries).

- Consequently, the method fails when the particulate flow is two or four way coupled, as the flow resolution around the particles is required to accurately describe the particle motion.

- This approach also breaks down at lower density ratios as the unsteady effects (such as Basset history and added mass effects to name a few) become important, meaning that the flow around the particle also needs to be resolved.

In-spite of these the Euler-Lagrange method can be used to study macro-scale (i.e transport across a monolith channel) deposition of PM aerosols, and can be used to assess the deposition efficiency of particular monolith designs. However, it cannot be used to study the critical pore diffusion phenomena that are fundamental to designing the next generation of PM mitigation devices.

4.2 Immersed boundary-FSI method: True DNS

The Euler-Lagrangian treatment is a convenient way of accounting for macro scale PM deposition in the channels of exhaust after-treatment devices. However, it still lacks the capability to inherently resolve the fluid-particle and particle-particle coupling due to a certain degree of modelling that is involved while setting it up. Hence, this framework cannot be used to study pore deposition of PM aerosols, a critical phenomenon to designing DPF's. One then has to resort to an approach in which the interaction between the particles and the gas, the boundaries of the flow and other particles can be accurately handled (i.e. is resolved and not modelled).

There are several techniques available for the complete DNS of such dispersed multiphase flows, such as front-tracking (FT), Immersed boundary (IB), Volume of fluid (VOF) etc. In this work, as an example we utilize an Immersed boundary method to develop a (continuum based) multiphase DNS framework to study PM deposition. The fundamental idea behind this framework is to couple the extended Langevin description of the particle (as formulated in Eq. 3.4) with a Cunningham correction to account for reduced momentum exchange between the phases (due to rarefaction) as shown in Eq. 3.3, to describe the diffusion of a spherical nanoparticle in an unbounded channel. The details of this framework are briefed below, beginning with a general overview on Immersed boundary methods.

4.2.1 Immersed boundary methods: A general overview

The immersed boundary methods are a class of numerical techniques employed in the computational fluid dynamics (i.e. numerical solutions to the Navier Stokes equations Eq. 2.1 using for e.g. finite volume discretization) of complex flow systems that greatly simplify the spatial discretization demands. This method, originally proposed by Peskin [66] to simulate cardiac mechanics and the associated blood flow, solves the governing equations in a Cartesian grid that does not conform with the complex geometries of the simulated system. In essence, the object around which the flow has to be assessed, is *immersed* in a standard cartesian flow grid, and its presence is accounted for by slightly modifying governing the Navier-Stokes equations. It should be noted that a surface grid still has to be generated for the immersed body (IB), however the volume grid on which the actual governing equations are solved for can be generated with no-regard to this surface grid [56]. The main advantages of such a treatment are as follows -

- Using a Cartesian grid can significantly reduce the per-grid-point operation count due to the absence of additional terms associated with grid transformations.

- On a non-body conforming grid, complexity and quality are not significantly affected by the complexity of the geometry

- Including body motion in IB methods is relatively simple due to the use of a stationary, non-deforming Cartesian grid

- Dynamic refinement around the immersed object is permissible meaning that the accuracy is increased at a minimal computational overhead.
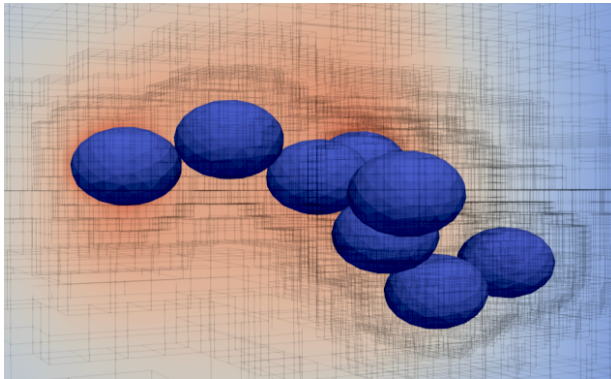
Figure 4.2: *IB simulation of a fractal soot particle: Note that there is no need for a body conforming mesh as the surface mesh (colored in blue) of the sphere cuts through an adaptive Cartesian octree background grid on which the discretized Navier-Stokes equations are solved (Eq. 2.1).*

Incorporating the presence of the IB in the Navier-Stokes equations is the primary challenge in setting up this framework. Usually this modification takes the form of a

source term (or forcing function) in the governing equations that reproduces the effect of the boundary. This is usually done in one of the following ways -

- Continuous forcing: the source term is introduced into the continuous equations (i.e. prior to the discretization) around the vicinity of the IB

- Discrete forcing: the source term is only introduced in the discretized equations around the vicinity of the IB (typically within the IB)

- Implicit forcing: there is no source term introduced into the equations. Instead, a boundary condition is used to constrain the velocity at the IB surface so that the correct behaviour is reproduced.

The continuous forcing approach is very attractive for flows with immersed elastic boundaries, and was originally envisioned by Peskin for the coupled simulation of blood flow and muscle contraction [66]. In this method the IB is represented as a set of elastic springs whose locations are tracked in a Lagrangian framework by a collection of massless points that move with the local fluid velocity. The effect of the IB on the surrounding fluid is essentially captured by transmitting the elastic stress (calculated using Hooke's law) to the fluid through a localized forcing term in the momentum equations [56]. This forcing is however distributed over a band of cells around each Lagrangian point (based on the discrete Dirac delta function). Consequently, this approach poses challenges for rigid bodies as the forcing terms are not easy to implement at a rigid limit. Moreover, due to the smoothing of the forcing term a sharp representation of the IB is not available. Consequently, this method is explicit and first-order accurate and unstable.

Hence, for dealing with sharply defined rigid bodies (as we do in this work), a better forcing alternative is desired. This can be fulfilled by employing a discrete (or non-distributive) direct forcing approach that adds the requisite source terms in the vicinity of the IB. Despite being second order accurate, this approach is only explicitly formulated and can be unstable for unsteady flows. Alternately, the implicit forcing approach can also be used to treat bodies with sharply defined edges (as we do in this thesis). In this method, the velocity at the IB is constrained by an implicitly formulated immersed boundary condition (IBC) (that is second-order accurate). This unique and stable treatment is central to the efficiency and accuracy of the multiphase DNS framework used in this thesis and will be discussed briefly in the following section.

4.2.2   Mirroring immersed boundary method

Let us revisit the governing equations for the flow around the immersed boundaries i.e. the continuity and momentum equations for in-compressible flow, the Navier–Stokes equations –

$$\frac{\partial u_j}{\partial x_j} = 0,$$

$$\frac{\partial (\rho u_i)}{\partial t} + \rho u_j \frac{\partial u_i}{\partial x_j} = -\frac{\partial p}{\partial x_i} + \frac{\partial}{\partial x_j}\left(\mu \frac{\partial u_i}{\partial x_j}\right) + f_i,$$

(4.1)

where f_i represents any external source term. Note that Eq. 4.1 is the final form obtained from the more universal Eq. 2.1. This set of equations is solved together with the implicit Dirichlet IB condition,

$$u_i = u_i^{ib},$$ (4.2)

which sets the velocity of the fluid to the local IB velocity. In the mirroring IB method, the velocity is set by an implicitly formulated second-order accurate immersed boundary condition. In this method the interior cells and the cells close to the surface are identified, see Figure 4.3.
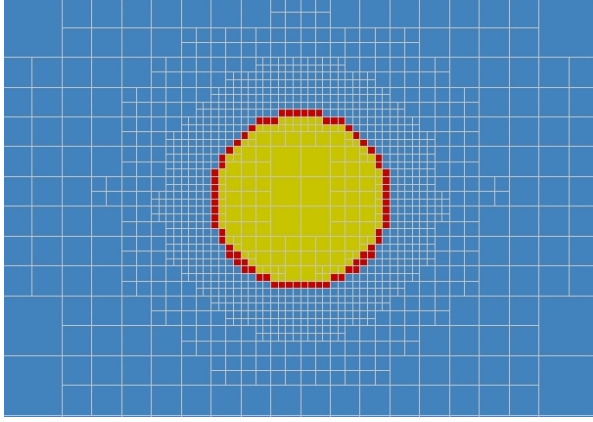
Figure 4.3: *2D view of the adaptive dynamic grid refinement around an immersed spherical soot particle (diameter of 400 nm). Cell types shown are exterior (blue), interior (yellow) and mirror or IB cells (red).*

For the mirroring cells, that lie close to the surface, their centers (mi) are geometrically mirrored over the local IB to the exterior points (e) c.f. Eq. 4.3. By mirroring the velocity field over the IB, second order accuracy is achieved.

$$u_i^{ib} = \frac{u_{mi} + u_e}{2}.$$ (4.3)

Typically, the exterior points do not coincide with a grid point, hence implicit tri-linear interpolation is adopted. When the velocity field is mirrored over the IB a fictitious velocity field is generated. To fulfill the continuity equation, this field needs to be replaced by the IB velocity in all flux calculations (note that the velocity within the IB is not used). A more detailed description of the method is available in [50, 51]. It should be noted that in the current method the total force (acting on the IB) is given by the surface integral of the total stress tensor (c.f. Eq. 2.2 consisting of pressure and viscous contributions) over the IB, as follows -

$$F_{IB} = \int_{IB} \left(-p\delta_{ij} + \tau_{ij} \right) n_j dS = \int_{IB} \left(-p\delta_{ij} + \mu \left(\frac{\partial u_i}{\partial x_j} + \frac{\partial u_j}{\partial x_i} \right) \right) n_j dS,$$ (4.4)

and the corresponding torque on the IB is estimated using -

$$T_{IB} = \int_{IB} \mathbf{r} \times \boldsymbol{\sigma} \cdot \mathbf{n} dS. \tag{4.5}$$

Here $\mathbf{r}$ is the position vector of the IB and σ is synonymous with σ_{ij} in Eq. 2.2 i.e the fluid stress tensor for a surface S with normal $\boldsymbol{n}$. Further, a trapezoidal rule is used for integrating the stresses and torques on the IB. The IB method described above has been extensively validated and used for the DNS of complex multiphase flow phenomena [71, 27, 28, 49, 1, 34, 85, 18, 35].

4.2.3   Coupling the IB method with Brownian dynamics

In the previous sections we have established the basis of our IB based continuum multiphase DNS framework. In this section we handle the application in question, i.e. the diffusion of a spherical PM in an unbounded channel. In this study the particle sizes are in the nanoscale and therefore, the non-equilibrium behaviour described in the earlier sections need to be accounted for. Since we use a continuum framework, similar considerations about its applicability as in Section 3.1.2 can be extended towards the IB-framework as well (i.e. we should account for the reduced momentum transfer between the phases using the Cunningham correction (C_c in Eq. 3.5)). Further, some additional molecular phenomena that affect the particle diffusion dynamics (such as Brownian behaviour) are absent in a continuum description (as they have been averaged out while setting up the equation system 2.1). The Langevin equation Eq. 3.1 indicates that we can incorporate the relevant Brownian fluctuations by including a stochastic forcing term in our governing equations (either for the particle, fluid or both). Out of these, the two most viable alternatives (for handling non-equilibrium fluctuations) are briefly described below -

Stochastic forcing of the fluid: Landau and Lifshitz approach

The first possibility is to include the stochastic fluctuations only within the deterministic fluid description (by adding stochastic fluxes to the stress tensor) in order to reproduce the relevant non-equilibrium Brownian behaviour. This constitutes a group of methods referred to as the fluctuating hydrodynamic approach of Landau and Lifshitz [42] which is derived using the fluctuating-dissipation theorem of statistical mechanics applicable at mesoscopic scales [61, 29].

$$\frac{\partial \rho}{\partial t} + \frac{\partial (\rho u_j)}{\partial x_j} = 0$$

$$\frac{\partial (\rho u_i)}{\partial t} + \frac{\partial (\rho u_i u_j)}{\partial x_j} = -\frac{\partial p}{\partial x_i} + \frac{\partial (\sigma_{ij} + \Sigma)}{\partial x_j} \tag{4.6}$$

where Σ is the non-equilibrium fluctuations captured through random stresses modelled (stochastic momentum flux) as -

$$\Sigma = \sqrt{\eta k_B T}[\upsilon(r, t) + \upsilon(r, t)^T], \tag{4.7}$$

with $\upsilon(r, t)$ is a standard Gaussian white noise tensor field with uncorrelated components δ-correlated in space and time.

It should be noted that the LLNS equations are stochastic partial differential equations that reduce to the Navier Stokes equations (Eq. 2.1) in the limit of large volumes. The validity of the Landau–Lifshitz Navier–Stokes (LLNS) equations (c.f. eq. 4.6) for non-equilibrium systems has been assessed extensively in [22] and verified using molecular dynamics simulations by Mansour et.al. [48]. Further, the LLNS based methods have been used predominantly in liquid-solid rarefied systems, where in the breakdown of continuity (i.e. the traditional Navier- Stokes equations) occurs at considerably smaller scales [23]. Hence, no additional correction for the hindered momentum transfer due to rarefaction needs to be included, which is not the case in gas-solid rarefied systems. Hence, this approach has successfully been incorporated in several numerical methods that describe dynamics of colloidal particles in a liquid [26, 21, 15, 5, 40, 47, 14].

Although the fluctuating hydrodynamic approach has found utility in Brownian particle dynamics studies, there are still some bottlenecks associated with its implementation in general finite volume or finite element based DNS frameworks. The main difficulty is in devising a discretization scheme for the stochastic differential equation primarily because of the correlation between the form of the required fluctuation-dissipation relations and the choice of scheme [14]. Further, finite-volume discretizations naturally impose a grid-scale regularization (smoothing) of the stochastic forcing. Moreover, the non-linear LLNS equations are ill-behaved stochastic partial differential equations that are challenging to integrate [84]. Finally, and most crucially, employing the LLNS equations to describe gas-solid rarefied flow systems is still heavily debated particularly due to the higher Kn encountered in these systems. Moreover, due to the higher particle-fluid density ratios encountered in typical exhaust gas after-treatment systems, a Langevin based approach is more founded due to the prevalence of quasi-steady forces (i.e. unsteady effects such as history and added mass forces are negligible). Hence we will limit ourselves to the forcing the particle equation of motion in this thesis.

Stochastic forcing of the particle: Extended Langevin approach

The inclusion of Brownian fluctuations directly on the particles appears more intuitive and more parallel to the fundamental Langevin equation based methods such as Brownian or Stokesian dynamics [20, 8], as opposed to forcing the fluid. The most straightforward way is to use Eq. 3.1 to describe the particle dynamics. This is equivalent to solving the particle equation of motion (Eq. 3.4) with a stochastic forcing (as described by [83]) term. Hence, the easiest way to incorporate the Brownian fluctuations in a continuum based multiphase DNS framework is to directly incorporate the necessary stochastic behaviour within the particle equation. This is done by incorporating the total hydrodynamic force from the IB method in the Ounis and Ahmadi model (Eq. 3.4). This coupling is one of the novelties of the proposed continuum IB based multiphase DNS method. It should be noted that the method is only valid as long the Langevin treatment has a sound basis (i.e. PM aerosols have high particle-fluid density ratios and therefore can the unsteady effects

be neglected).

Consequently, the particle motion is governed by the conservation of linear and angular momentum (Eqs. 4.8 and 4.9). For a particle with mass m_p, translational $\mathbf{u_p}$ and angular velocity $\boldsymbol{\omega_p}$, moment of inertia $(\boldsymbol{J})$ and including the stochastic forcing $\mathbf{F_{Brownian}}(\mathbf{t})$ (c.f. Eq. 3.9), this is given as:

$$m_p \frac{d\mathbf{u_p}}{dt} = \frac{F_{IB}}{C_c} + \mathbf{F_{Brownian}}(\mathbf{t}), \tag{4.8}$$

$$\mathbf{J} \frac{d\boldsymbol{\omega_p}}{dt} = T_{IB} - \boldsymbol{\omega_p} \times \mathbf{J} \cdot \boldsymbol{\omega_p}, \tag{4.9}$$

Thus we have a physically consistent way of including both Brownian fluctuations along with decreased momentum exchange due to rarefaction (using the Cunningham correction Eq. 3.3) in any given multiphase DNS framework.

4.2.4 Immersed Boundary Octree Flow Solver: IPS IBOFlow

In this work, we use the multi-phase flow solver `IPS IBOFlow`, developed at Fraunhoffer-Chalmers Research Centre (FCC). This solver utilizes the previously described mirroring immersed boundary method (c.f. Section 4.2.2) to efficiently handle the moving particles. In the solver, the continuity and momentum equations are discretized and solved on an adaptive Cartesian octree grid [2], c.f. Fig 4.2 (that can be dynamically refined and coarsened). This ability to locally refine the computational mesh around the immersed boundaries is one of the highlighting characteristics of this flow solver. Figure 4.3 illustrates this local refinement in the case of an immersed spherical particle (representing an ideally shaped soot particle of diameter 400 nm) along with the corresponding cell types.

The pressure-velocity coupling in Eq. 4.1 is handled using the segregated SIMPLEC method [17] which first approximates the momentum equation with an estimated pressure field, and then corrects the pressure by employing the continuity equation. All variables are stored in a co-located grid arrangement (meaning that the variables such as pressure, velocity etc. are stored at the cell centres). The Rhie-Chow [68] flux interpolation is used to suppress pressure oscillations. `IPS IBOFlow` is coupled with `LaStFEM`, which is an in-house finite-element (FEM) based rigid body solver [72] developed at FCC. This solver can resolve the particle short range dynamics (i.e fluid structure interaction FSI of rigid objects) to fully resolve the particle diffusion dynamics (i.e. at least two-way coupled, and has the capability to be extended towards a four-way coupled framework). From here on this coupled framework will be referred to as the IB-FSI framework. The FEM solver computes the rigid body motion by solving the linear and angular momentum conservation equations 4.8 and 4.9. Note that Eq. 4.8 is an extension of the original Ounis and Ahmadi treatment of aerosol particulates(c.f. Eq. 3.4) with a major difference that we include the resolved fluid hydrodynamics in this conservation equation.

The Newmark time scheme [60] is used for the temporal integration of the SDE. In this method, acceleration, velocity and displacement at time $t = t^{n+1}$ is obtained as a

function of the values at $t = t^n$ (which is always known), by assuming a linear acceleration during that small time step. This one-step semi-implicit method can be represented by the following sets of equations -

$$\dot{u_p}^n = \dot{u_p}^n + \frac{\Delta t}{2}\left(\ddot{u_p}^n + \ddot{u_p}^{n+1}\right) \tag{4.10}$$

$$u_p^{n+1} = u_p^n + \Delta t\dot{u_p}^n + \frac{1-2\beta}{2}\Delta t^2\ddot{u_p}^n + \beta\Delta t^2\ddot{u_p}^{n+1} \tag{4.11}$$

This scheme is also unconditionally stable with β a tuning parameter that has a default value of 0.25 (the constant average acceleration method) [60]. The scheme is also confined within the Itô interpretations [33] of a stochastic integral, and hence can be safely used to solve the SDE governing the particle motion (Eqs. 4.8 and 4.9). A partitioned approach is employed to solve the coupled rigid body - IB problem. The grid and assembly are fully parallelized on the CPU and the resulting large sparse-matrices are solved on the GPU with a Algebraic Multi-Grid (AMG) solvers [59].

This extension of the original Ounis and Ahmadi model towards a continuum framework, is the major contribution from this work, and to our knowledge this is the first multiphase DNS method that can handle the dynamics of aerosol nano-particles in rarefied flows (i.e both Brownian dynamics and the hindered momentum transfer to break down of continuum theory are fully accounted for). Further using such a rigid body solver would mean that the we already have the infrastructure to account for sub-grid particle-particle and particle-wall interactions as well (these can be included through the widely available collision, lubrication models etc.). Additionally, as we use an IB method the need for a body fitted grid is redundant, meaning that we can easily simulate complex particle shapes. Moreover, this framework can also resolve particle deformation if needed (coupling between hydrodynamics and structural mechanics), however in this thesis we limit ourselves to simulations of rigid PM aerosols. It should be noted that there are some inherent limitations with the IB-FSI framework as well, some of these are listed below -

- This DNS framework is computationally expensive particularly for simulating long-term statistics of Brownian motion.

- Currently, the IB-FSI framework can only be used with unbounded flows, mainly because the closures to describe rarefaction effects near wall bounded regions are currently lacking (meaning the method will be inaccurate for near wall particulate flows).

- The framework is also very sensitive to the particle-fluid density ratios. This is because both the coupling schemes between the rigid body solver and the IB solver and the inherent Langevin equations are effected by the density ratios. This framework in in its current form will breakdown at low particle-fluid density ratios.

4.3 Numerical setup

We now provide an overview of the numerical setup employed in the simulations along with its validation. We describe the final numerical setup that has been used for the simulations including brief accounts on the grid and time-step convergence. A spherical particle is released at the center of our domain (which is symmetric on all sides) and is subject to both the hydrodynamic forces (from the DNS) and the stochastic Brownian forcing (extended Langevin approach). In this IB framework, the Navier-Stokes (NS) equations (c.f. Eq. 2.1) are discretized on an adaptive octree grid. This grid is further used to calculate the fluid stresses on the solid as shown in [51, 50] and in Eq. 4.4. These surface integrated stresses are then coupled with a finite-element based rigid body solver [72] that can resolve the short range particle dynamics. A schematic of the simulation domain is shown in Fig 4.4. The simulation conditions (similar to the Lagrangian benchmarks) are further listed in Table 4.1.
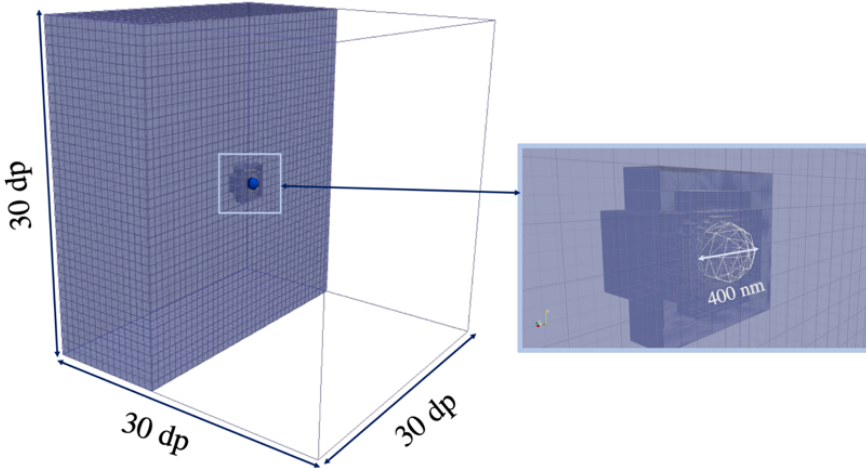
Figure 4.4: *Schematic of the simulation domain employed in the particle diffusion studies (Inset: Octree grid around the 400 nm particle).*

4.3.1 Validation of the framework

The IB-FSI framework used in this work is first validated using a standard Stokes settling case for a spherical aerosol particle (with a diameter of 400 nm) accelerated by a constant force in the negative z-direction. For such PM systems, it is common to assume a density of 1000 kg/m^3 for all relevant particle sizes (as proposed by Kittelson [39]). This force was chosen so as to accelerate the particle to its root mean square velocity (V_{rms}). A detailed temporal and grid convergence was undertaken in order to show the sensitivity of the multiphase DNS method to the temporal and spatial discretization employed. The results from this assessment are shown in Fig. 4.5 below. These results are presented in terms of the non-dimensional velocity ($V_z^{simulation}/V_z^{analytical}$) and non-dimensional

Table 4.1: Simulation settings and fluid properties

Condition	Case: Grid convergence	Case: Time convergence	Case: Diffusion
System size (l x w x h), *microns*	10 x 10 x 13	10 x 10 x 13	10 x 10 x 13
Particulate phase: Spherical soot particle			
Diameter, *nm*	400	400	400
Density, kg/m^3	1000	1000	1000
Fluid phase: Air			
Density, kg/m^3	1	1	1
Dynamic viscosity,*Pa.s*	1.8e-5	1.8e-5	1.8e-5
Simulation settings			
Spatial resolution, *cells/diameter*	12, 24, 48, 96	24	24
Temporal resolution, *s*	$1/100\tau_p$, $1/200\tau_p$, $1/400\tau_p$, $1/800\tau_p$	$1/10, 1/35, 1/70, 1/100, 1/200\tau_p$	$1/200\tau_p$

time(t/τ_p). Note that we describe the acceleration of the particle towards it's terminal settling velocity. Further, the relative error across the temporal and spatial resolutions in this study are summarized in the Table 4.2. This error between the simulations and the analytical results is calculated using -

$$Relative\ error = \frac{V_z^{analytical} - V_z^{simulation}}{V_z^{analytical}} * 100. \tag{4.12}$$

Table 4.2: Spatial and temporal convergence for a spherical particle of density 1000 kg/m^3 accelerated by a constant force in the -ve Z direction after 10 particle response times (τ_p). The values highlighted in *red* are the chosen spatial and temporal resolutions for the DNS framework.

(a) Grid convergence

Grid resolution	error (%)
12 cells/dia	15.2%
24 cells/dia	5.2%
48 cells/dia	3.3%
96 cells/dia	2.1%

(b) Temporal convergence

Temporal resolution	error (%)
$\tau_p/10$	18.8%
$\tau_p/35$	7.9%
$\tau_p/70$	3.6%
$\tau_p/100$	2.2%
$\tau_p/200$	0.9%

A variety of grid resolutions were tested, at a fixed Courant number ($C = \frac{u\Delta t}{\Delta x}$) based on an initial temporal resolution of $\tau_p/100$ (i.e. the coarsest spatial resolution of 12 cells/diameter uses a temporal resolution of $\tau_p/100$). The successively finer spatial resolutions employ a correspondingly finer temporal resolution so as to maintain the same Courant number. A rule of thumb in such multiphase DNS simulations is to have at least 20 cells per diameter as the resolution, and this is realized in our assessments as well (see c.f. Fig 4.5a). The solution is clearly grid independent if a minimum resolution of 24 cells/diameter is maintained. Moreover, although the reported relative error does decrease with a finer resolution (as expected), it creates an increased computational overhead. Hence, in order to counter-balance computational demands and the expected accuracy, a grid resolution of 24 cells/diameter (with a relative error of $\approx 5.0\%$) will be used as the basis for all the studies presented in this thesis. Next, the sensitivity of the IB-FSI framework to temporal discretization is shown in Fig. 4.5b. It is quite evident that the chosen simulation time step (represented in terms of the particle response time τ_p) has a direct impact on the accuracy of the results, with a temporal resolution of at least $\tau_p/70$ needed to produce convergent solutions. Since the computational overhead from the time step demands are not as severe as those from the grid requirements, we select the finest possible temporal resolution of $\tau_p/200$ (with a relative error of $\approx 0.9\%$) as a minimum requirement that will always be met in this thesis. As is evident, the error from the numerical framework has to be kept minimal if we are to perform a *true* DNS of the particulate aerosols, and this constraint is maintained throughout this work.
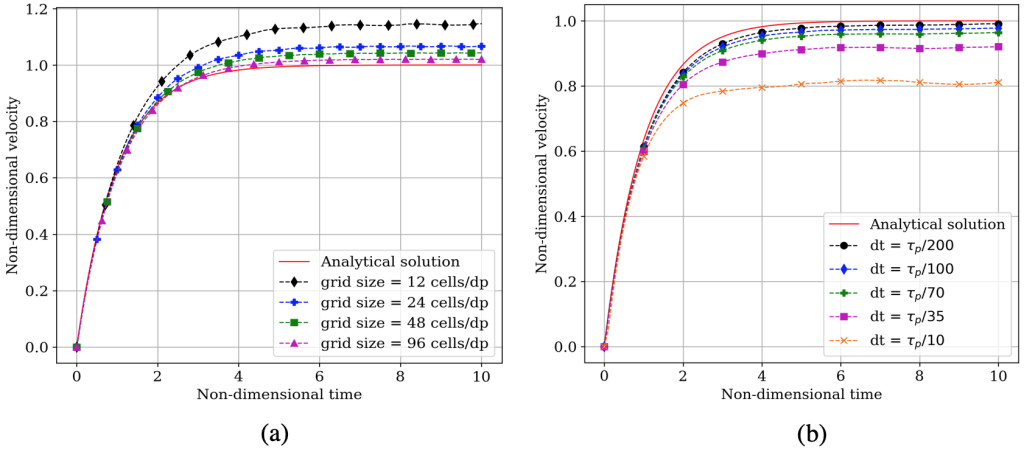

Figure 4.5: *Sensitivity assessments on the IB-FSI framework: a) Grid and b) Temporal convergence after 10 response times. The red lines (——) represent the analytical Stokes settling under a constant force in the -ve Z-direction (solved by integrating the particle equation of motion).*

4.3.2 Final simulation conditions

Based on the detailed sensitivity analysis on the IB-FSI framework, the following final choices are made for the numerical set-up. A grid resolution of 24 cells/diameter and a temporal resolution of $\tau_p/200$ would be used in all the results presented in this thesis. Further, the Brownian forcing is done every $\tau_p/10^{\text{th}}$ timestep to allow for a better resolution of the particle acceleration. The diffusion of a single spherical nanoparticle of diameter 400 nm is studied in an unbounded channel. The effect of particle-fluid density ratio on the diffusion dynamics would be studied with this numerical setup. The list of cases that have been studied are listed in Table 4.3.

In a multiphase DNS framework such as this, the hydrodynamic coupling is fully resolved (by integrating the fluid stresses on the surface of the particle) and not modelled (c.f. Section 3.1). Hence, in addition to steady and unsteady effects, the full hydrodynamic coupling would also include effects from the presence of flow boundaries as well as proximity to other particles. However, in this thesis we only wish to demonstrate a proof-of-concept of our universal framework (i.e. it can be used in any multiphase DNS setting). Hence, we only demonstrate unbounded Brownian diffusion at sufficiently high particle-fluid density ratios in Stokes flow as a first example.

Table 4.3: Cases simulated using the IB-FSI framework

Case	Particle/Fluid density ratio
DBP1	2000
DBP2	1000
DBP3	500
DBP4	100

4.4 Results: IB-FSI simulation of an ideal spherical soot particle (in an unbounded domain)

The IB-FSI framework is used to simulate the diffusion of a typical soot like spherical particle (with a size of 400 nm) in an unbounded channel (c.f. Table 4.3). These results are used as a base case to evaluate the overall performance of the framework, particularly as the Langevin equation for the particle (Ounis and Ahmadi model) will now include the fully resolved hydrodynamics (as opposed to a quasi-steady model such as Stokes drag) around the particle. It is expected that at such high particle-fluid density ratios, this treatment should easily extend towards this application with PM aerosols. This is mainly because, under these conditions, the unsteady effects are negligible (see Section 3.1.1), meaning that the solution to the Langevin equation should be similar to the benchmark tests. Note that for this proof-concept we assume an inert particle and that reactivity can easily be added if needed.

4.4.1 Diffusion of a spherical soot-like particle of density 1000 kg/m³

Some general results from the IB-FSI framework simulations (in terms of particle trajectories and MSD^*) are presented in Fig. 4.6. These predictions from the framework are in excellent agreement with the benchmark Lagrangian one-way coupled simulations, capturing the transition from the ballistic to the diffusive regime (as detailed earlier c.f. 3.3.1). This close correspondence can be considered as a qualitative validation of the performance of the framework. Further, the results are within the variability reported in the benchmark simulations (across different trajectories or 5 different random seeds). These close comparisons in the MSD^* can be further appreciated by examining the particle positions and velocities between the one-way and two way coupled treatments (c.f. Fig. 4.7). Note that the same sequence of random numbers, as those used in the benchmark study, are used in the IB-FSI simulations as well.
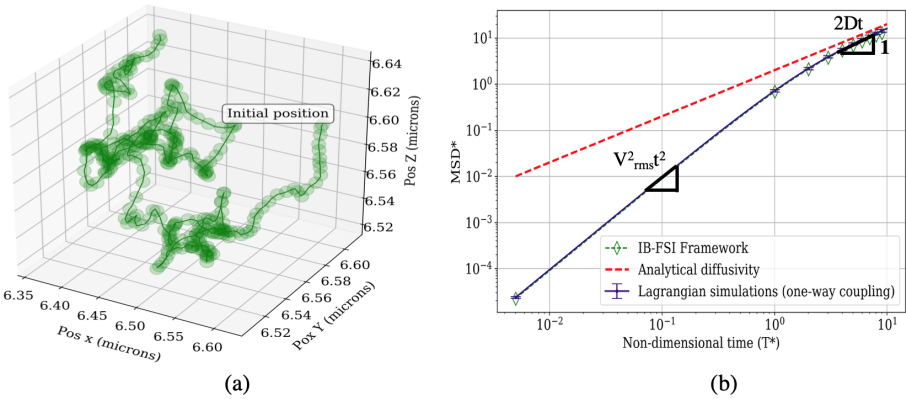

Figure 4.6: *Particle diffusion dynamics (IB-FSI simulations): a) Trajectory of a 400 nm diameter particle (with density 1000 kg/m³) and b) Non-dimensional MSD after a lag time of 10 response time units across different density ratios after 150 response times (the slopes indicate the ballistic and diffusive regimes). The red dashed lines (- - -) represent the Einsteins analytical diffusivity (Eq. 3.10).*

4.4.2 Effect of density ratio on diffusion dynamics

The IB-FSI framework is now used to perform a variety of numerical experiments that would evaluate the particle diffusion dynamics as a function of particle-fluid density ratio (c.f. Table 4.3). The aim of this assessment is to demonstrate the applicability of our framework to study aerosols of particles with soot-like densities. This broad applicability is shown in the Fig. 4.8a, where in the corresponding MSD^* values across realistic soot-particle densities compare very well with the benchmark Lagrangian results. Note
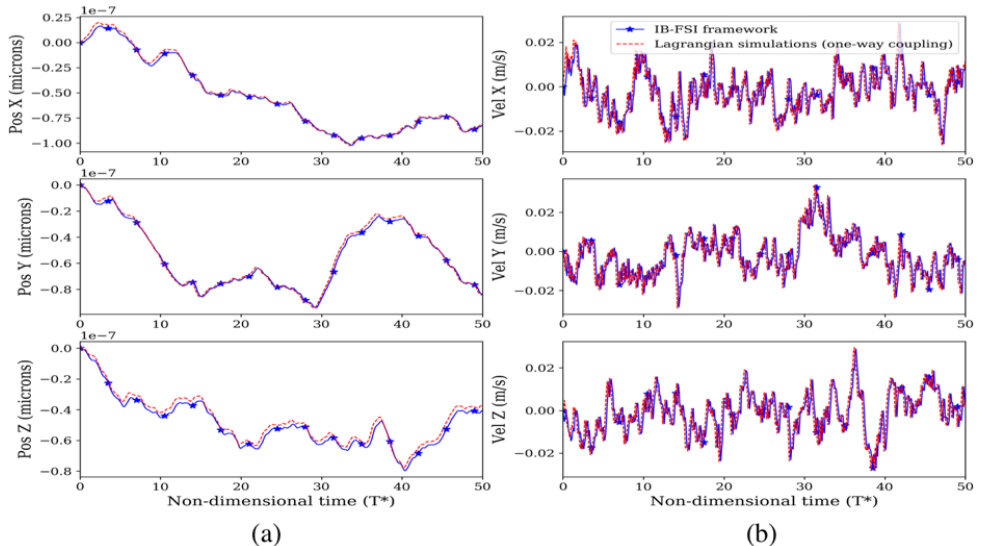
Figure 4.7: *Particle diffusion dynamics (IB-FSI simulations): a) Position and b) Velocity of a 400 nm diameter particle (with density 1000 kg/m³) after 150 response times.*

that there is negligible variation across the simulated density ratios. Further, the Gaussian nature of the stochastic forcing in Eq. 3.9 would mean that the consequent stochastic process is Markovian in nature. Hence, the auto-correlation function (v_{acf}) for the particle velocities, given as –

$$v_{acf} = \langle \mathbf{v(0)} \cdot \mathbf{v(t)} \rangle = \frac{1}{N} \sum_{n=1}^{N} \left(\mathbf{v(0)} \cdot \mathbf{v(t)} \right), \qquad (4.13)$$

decays with an exponential tail, as shown in Fig. 4.8b. This classical result for Brownian particles [77] with sufficiently high density ratios, is a further validation of the applicability and performance of our framework. Note that the analytical exponential decay in Fig. 4.8b is slightly offset at the beginning from the decay of the v_{acf} of the simulated particles. This is attributed to the ballistic behaviour which is accounted for in the multiphase DNS treatment. Einstein's analytical behaviour (Eq. 3.10), on the other hand, does not include this initial ballistic phase and is purely diffusive. Nevertheless, the two sets of curves do match with each other after this initial ballistic phase.

We further evaluate the accuracy of the current framework by comparing the root-mean squared velocities (V_{rms}) of the particle across the different particle-fluid density ratios. This is a good metric to judge if the right physics are being captured in our framework (i.e. if the stochastic behaviour is correctly resolved). The analytical V_{rms} (given as $\frac{k_B T}{m_p}$), is a function of the particle density, and this trend is presented in the Fig 4.9 (as the particle is lighter it will be easily accelerated by molecular collisions, meaning that it would have an increased V_{rms} value). It is quite apparent that the IB-FSI framework
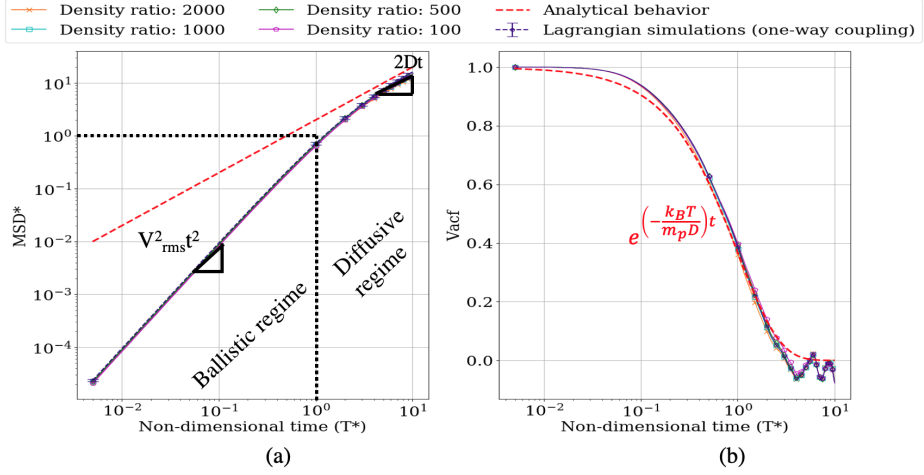
Figure 4.8: *Particle diffusion dynamics (IB-FSI simulations): a) MSD* variation and b) Averaged velocity auto-correlation function (v_{acf}) across different particle-fluid density ratios after 500 response times (all the Lagrangian benchmarks are represented by one curve). The red dashed lines (**- - -**) represent the Einsteins analytical behavior (Eq. 3.10).*

closely follows the analytical trend. Note also that the Lagrangian benchmarks closely mimics the analytical trend, which is a further confirmation that the extended Langevin equations of Ounis and Ahmadi (Eq. 3.4) offer reasonable benchmark limits for comparing the performance of our framework. The relative difference between the V_{rms} values from the IB-FSI framework and the analytical values are listed in Table 4.4 to the show a quantitative metric of accuracy (for the the framework), given as -

$$Relative\ error = \frac{V_{rms}^{analytic} - V_{rms}^{simulation}}{V_{rms}^{analytic}} * 100. \tag{4.14}$$

Table 4.4: Relative error in the IB-FSI framework (calculated using the relative difference between the V_{rms} values from the IB-FSI framework and the analytical values) after 150 response times

Case	Particle/Fluid density ratio	error (%)
DBP1	2000	4.5%
DBP2	1000	3.6%
DBP3	500	4.4%
DBP4	100	5.1%

We report a maximal 5% error with this framework , synonymous with the error reported for our chosen spatial resolution in the validation studies c.f. Section 4.3.1. This is an acceptable margin, and further shows the feasibility of this DNS framework.
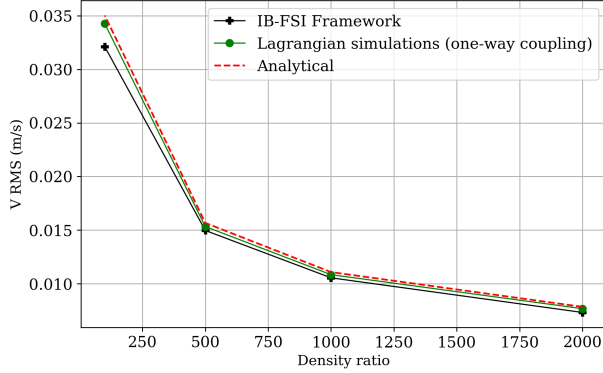
Figure 4.9: *Comparison of V_{rms} between the IB-FSI framework, Lagrangian benchmark and Analytical results across density ratios between 2000 and 100 kg/m³ after 500 response times. The red dashed lines (- - -) represents the Analytical values.*

4.4.3 Some anomalies: Diffusion at low particle-fluid density ratios

The feasibility of the IB-FSI framework to resolve the relevant particle dynamics of relatively heavy particulates (typically in the range 2000 and 100 kg/m³) has been demonstrated in the preceding sections. There are however some limits to its applicability, at least in the current form. These limitations are determined by the particle-fluid density ratio of the simulated particulate aerosols. The extended Langevin equation (Eq. 3.4) in its current form cannot be used to describe the dynamics of lighter particles (density <10 kg/m³), mainly because the friction (drag) on the particle has not reached a steady state after having received an impulse from the fluid (i.e. the developing hydrodynamic motion is not fully described by the steady Stokes drag) [30]. Thus the fluid inertia (including unsteady effects) must also be included along with the particle inertia (in the stochastic forcing term Eq. 3.9) to describe the particulate dynamics accurately. This deficiency with the Langevin treatment was first noted by Rahman [67] and Alder and Wainwright [3] in some simulations of Brownian motion in a liquid, when they reported a long-tailed decay in the velocity correlation function v_{acf} (as opposed to the exponential decay reported in this work c.f. Fig. 4.8). This would mean that the particle motion is not δ-correlated in time any more, and deviations from true Brownian behaviour will be exhibited as shown in Fig. 4.10a and b.

Fig. 4.10 demonstrates the diffusion of spherical particles with density <10 kg/m³. These cases show the failure of the IB-FSI framework (based on the extended Langevin treatment). Fig. 4.10b provides a more measurable metric for convergence towards Brownian behaviour. Here we plot the ratio between the diffusivity obtained from the simulations (D) and the Diffusivity (D_{phi}) set in the Brownian forcing term (3.9) of the extended Langevin equation over non-dimensional time. Ideally, this curve must approach unity (as we hope to get the Einstein's diffusive behaviour using the Langevin equation). Slight
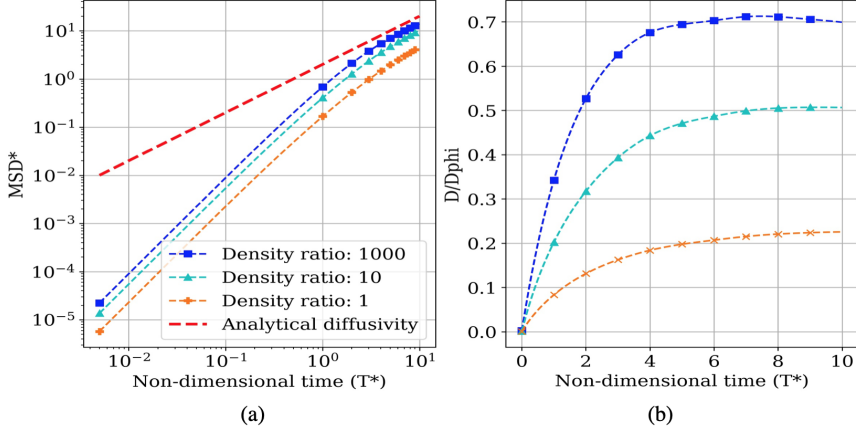
Figure 4.10: *Particle diffusion dynamics (IB-FSI simulations): a) MSD* variation and b) variation of $\frac{D}{D_{phi}}$ which represents the convergence towards Brownian behaviour after 150 response times . The red dashed lines (- - -) represent the Einsteins analytical behaviour (Eq. 3.10).*

variations from unity are permissible, due to the inherent stochastic nature of the process, meaning that based on the chosen random seed the final process will fluctuate around unity (which is why an ensemble average over several trajectories/processes is desired for the exact description of Brownian dynamics). However, the behaviour noted for the curves with particle-fluid density ratio <10 clearly indicates that the particle dynamics can no longer be accounted for by solving only the Langevin equation of motion, as some of its inherent assumptions are violated. This deviation from Einstein's analytical behaviour can further be confirmed by evaluating the tail decay behaviour of the velocity auto-correlation function (v_{acf}) as shown in Fig . 4.11. Clearly, the simulations with a low-particle to fluid density have a slightly different tail decay than the the analytical exponential decay, indicating the failure of a pure Langevin description of the particle dynamics.

In-spite of these inherent deficiencies at the lower particle-fluid density ratios, our framework is still quite capable at handling the particle dynamics of soot like particles at realistic densities. The results presented as anomalies, are primarily used to establish the bounds in terms of applicability for our novel IB-FSI framework.

4.5 Extending the IB-FSI framework to study a real fractal soot-particle

The IB-FSI framework has been shown to accurately handle the Brownian dynamics of spherical soot particles (in unbounded domains), however in reality these particles have fractal morphologies. Our framework is also designed to handle such nuclei mode fractal aggregates. Since we employ a rigid body solver, the dynamics of these fairly
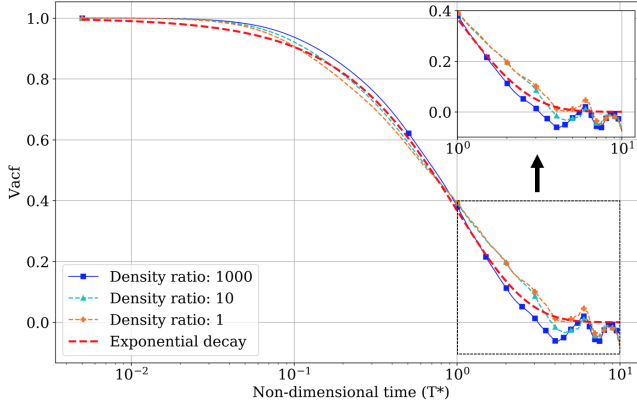
Figure 4.11: *Averaged velocity auto-correlation function (v_{acf}) from simulations at low particle-fluid density ratios (of 10 and 1 kg/m^3) compared with the simulation of a higher particle-fluid density ratio of 1000 kg/m^3 after 500 response times .The inset describes the deviation from the analytical exponential tail decay behavior at these lower density ratios. The red dashed lines (- - -) represent the Einsteins analytical behavior (Eq. 3.10).*

complex fractal aggregates can inherently be handled, provided the physics of the system (i.e. the drag reduction due to rarefaction (Cc in Eq.(3.5)) and Brownian dynamics) are consistently incorporated. This is the biggest challenge in extending the IB-FSI framework towards a real soot particle, particularly as the closures needed to account for the non-equilibrium behaviour would need a characteristic dimension. The fractal nature of the real aggregate would mean that this has to be accounted in an indirect way.

4.5.1 Fractal aggregate generation

The soot aggregates are formed from the smallest primary hydrocarbon particles (denoted the nuclei mode particles) that are formed during the combustion process. These increase in number as the exhaust gas passes through the aftertreatment system via a number of different nucleation mechanisms (including condensation of volatile substances from the gas phase). These nuclei mode particles are a few nanometers in size when they first appear and they thereafter grow to form fractal aggregates. Hence a detailed insight into the complex transport and deposition of these real aggregates in the pores and channels of a monolith can definitely aid in designing smarter materials and devices to capture PM more efficiently. Our novel framework represents the very first continuum-based numerical method that can resolve the dynamics of such irregularly shaped PM aerosols.

The first challenge in setting up such simulations is to account for rarefaction in particulate aerosols with *non-spherical particles*. These fractal aggregates can be described as entities composed of a number of contacting or partially coalesced primary spheres, where the number of primary spheres per entity (N) exhibits a power law relationship with the

entity's radius of gyration (R_g) [69, 41] given as -

$$N = k_f \left(\frac{R_g}{a}\right)^{D_f},$$ (4.15)

where a, D_f, and k_f are the the mean primary particle radius, fractal dimension (exponent), and fractal pre-factor, respectively. Based on this, we set-up the simulation of a typical soot particle as shown in Fig. 4.12. These fractal aggregates are generated using standard particle–cluster (PC) aggregation algorithms that have been implemented by Skorupski et.al [76]. These algorithms attach one spherical sub-unit to the growing cluster at each step of the aggregation process in such a way that the scaling law (Eq. 4.15) is fulfilled exactly at each step for prescribed values of the fractal dimension and pre-factor. The open-source program `FLAGE` (Fractal-Like Aggregate Generation Environment), developed by Krzysztof Skorupski ([75]) is used to create the corresponding aggregates. These are then post-processed in `Netgen` and `FreeCAD` to generate the required surface mesh (`stl`) of the object that will be used in the the IB-FSI framework.
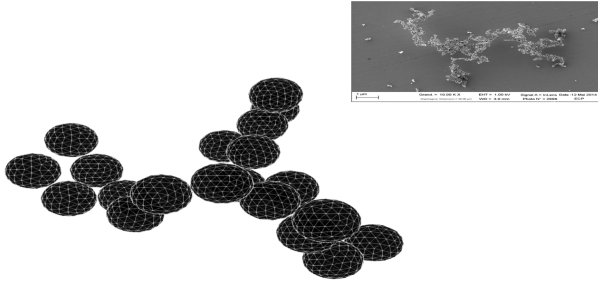

Figure 4.12: *A typical fractal-like soot aggregate with fractal pre-factor (k_f) 1.3 and fractal dimension (D_f) 1.78. Inset: SEM of a typical engine generated soot aggregate (figure adapted from [62]).*

4.5.2   Characterizing the fractal aggregate

Recently, Zhang et al. [86] proposed a simple algebraic expression for the orientationally averaged scalar friction factor (c.f. 3.5) of an arbitrarily shaped aerosol particle across the entire Kn range using high fidelity DSMC methods. They state that if the Kn of the fractal particle can be defined in terms of the hydrodynamic radius of the non-spherical particle (R_h) (as originally defined by Hubbard and Douglas [32]) and the the projected area (PA), as defined below -

$$Kn = \frac{\lambda \pi R_h}{PA},$$ (4.16)

a slip correction analogous to the one used for spherical particles (as in Eq. 3.3) can be used to describe the rarefaction. This would mean that the diffusive Kn is a shape-independent relation that describes the low-Reynolds number, low-Mach number, orientationally averaged drag force on arbitrarily shaped particles [86].
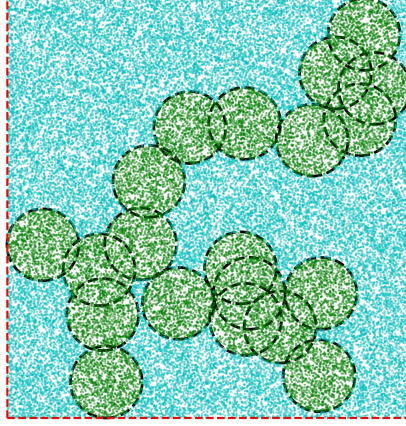
Figure 4.13: *Calculation of PA using Monte Carlo sampling: The Orthogonal projection of the aggregate (in the x-y plane) is indicated by the black dashed circles (- - -). P uniformly distributed points are sampled within a rectangle (box with red dashed lines - - -) that encloses this specific orientation of the fractal aggregate. Each sampled point is checked to determine whether it is inside (N_{in}) or outside (N_{out}) the projection of the particle shape. PA is calculated using Eq. 4.18, and this process is repeated for 10^4 orientations to obtain the orientationally averaged projected area PA.*

We extend this idea to describe the dynamics of the real soot particle using our IB-FSI framework. We use the algorithm described by Gopalakrishnan et al. [25] for calculating orientationally averaged R_h. First passage time simulations (developed by Torquato and co-workers [81]) of inertialess Brownian walkers are used to estimate the R_h value. More details about this method are available in the supplementary material of the work by Gopalakrishnan et al. [25]. As a brief summary, a visual representation of the algorithm is provided in Fig 4.14. Consequently, a walker can have only two fates; it can either collide with the aggregate or escape. The number of colliding (N_C) and non-colliding walkers (N_{NC}) are then used to estimate the R_h value as follows -

$$R_h = \frac{N_C}{N_C + N_{NC}} * R_{outer} \tag{4.17}$$

The projected area (PA) i.e. the maximum extent of the particle shape on an orthogonal projection plane, is calculated using a simple Monte-Carlo sampling technique. P uniformly distributed points are sampled from a rectangle (with area A) that encloses one specific orientation of the fractal aggregate completely (the value P is tuned for both high accuracy and optimal computation times). Each sampled point is checked to determine whether it is inside (N_{in}) the projection of the particle shape. The final PA for this specific

orientation is calculated as -

$$PA = \frac{N_{in}}{P} * A \tag{4.18}$$

This calculation is repeated for 10^4 orientations and the orientationally averaged projected area is calculated as the arithmetic mean of all these individual projected areas. An example of this Monte Carlo sampling method is shown for one particular aggregate orientation in Fig 4.13.
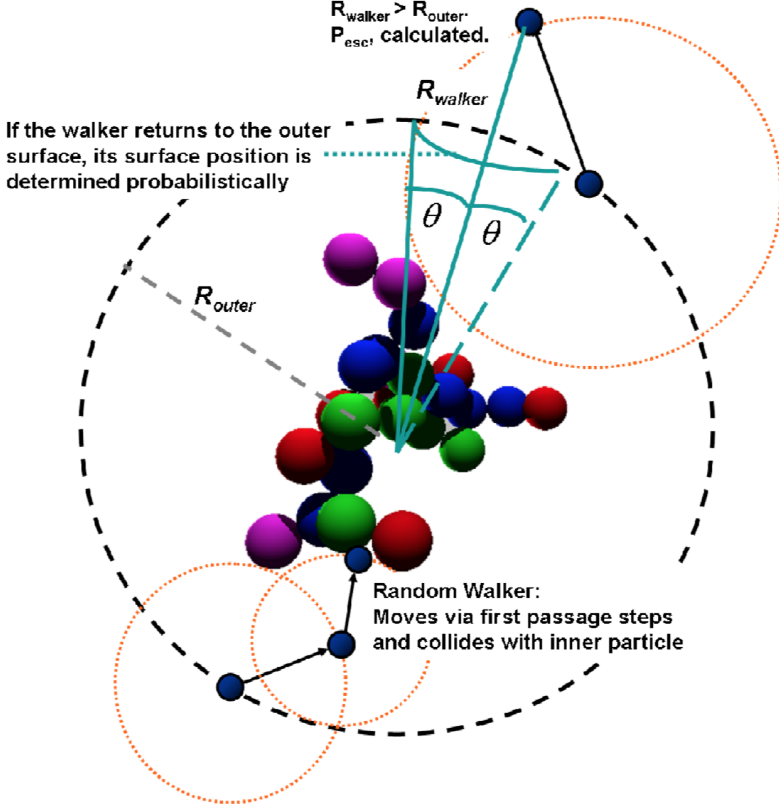
Figure 4.14: *Calculation of R_h using the algorithm proposed by Gopalakrishnan et al. [25]. An inertialess Brownian walker is released from the surface of a sphere with radius $R_{outer} >> R_g$ of the aggregate. This walker is then moved by first passage time simulations. Based on the motion two fates are assigned to the walker (i.e. it can collide or escape), and finally after n-steps the Brownian walker either collides or escapes. The number of colliding and non-colliding walkers are used to calculate R_h (figure adapted from [25]).*

4.5.3 Preliminary results

Based on these calculations, the corresponding dimensions of the soot aggregate that will be simulated are given in Table 4.5 below -

Table 4.5: Dimensions of the fractal aggregate

Dimension	value
D_f	1.78
k_f	1.3
R_h	174 nm
PA	$6.4e{-}14$ m^2

As a first assessment, we simulate the soot aggregate described in Fig. 4.12 and Table 4.5 using the IB-FSI framework. Currently, the rotational equation for the aggregate motion has not been solved, and we only look at the translational behaviour. The results presented are still in the early stages of development, nevertheless they are briefly described here to showcase the application of our novel IB-FSI framework to simulate real PM aerosols. In Fig. 4.15 we compare the pressure distribution around an aggregate and a spherical particle. This evaluation clearly shows the asymmetric distribution of the pressure contours around an aggregate. Such a result is extremely valuable to understanding the complex hydrodynamic phenomena around an aggregate. These results represent a preliminary assessment, and one of the continuing aims of this work is to extend these simulations with rotational asymmetry.
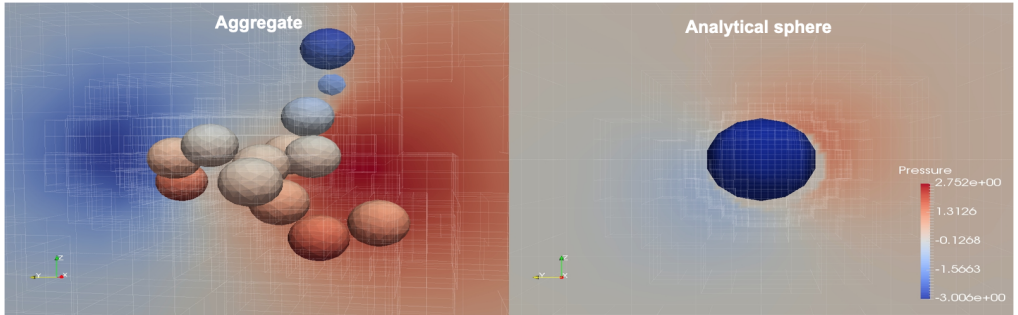
Figure 4.15: *Comparison between a fractal aggregate and a spherical particle: Pressure distribution around the particle. Note that the pressure distribution around the aggregate is asymmetric. (the particles are colored based on pressure).*

Thus, the building blocks for a universal multiphase DNS method that can handle the diffusion of PM aerosols under rarefied conditions has been established. This novel IB-FSI framework has shown promising capabilities and will be developed even further to accurately resolve the dispersion of fractal like soot aggregates (including the asymmetric rotational effects as well). Moreover, the fundamental idea behind this framework is easily transferable to any multiphase DNS technique, making this method truly *universal*.

Chapter 5
Concluding remarks

In this thesis, we have presented and discussed a suite of numerical tools (extending from single phase to multiphase descriptions of the system) for studying the deposition of particulate aerosols in conventional exhaust gas after treatment devices such as particulate filters. We have established that numerical methods and experimental assessments can be used to complement each other (i.e. by comparing the measured PM capture to a simulated one we were able to identify the real reactive nature of particulates), to obtain a heuristic overview of the complicated phenomena encountered in these systems. This led to the need for more rigorous numerical tools that can accurately resolve the prevalent physics in such systems. Consequently we have developed a novel multiphase DNS tool that is suitable to study the transport and deposition of real soot PM in the monolith channels of a conventional DPF. It should be re-iterated that the proposed numerical methods are universal and can be applied to any multiphase DNS framework.

Contributions from this work

We summarize the critical contributions from this work in terms of the aims that were originally stated in the beginning of the thesis (Section 1.3). These are listed as follows -

1. To use computational fluid dynamics based methods to study the movement and deposition of particulate aerosols in a monolith channel of a DPF (fully Eulerian single phase simulations assuming inert particulates).

   - Established the need for describing PM transport dynamics more rigorously by identifying the differences between experimental measurements and simulations (Eulerian convection-diffusion treatment) of the transport of soot particulates from a diesel engine in a conventional exhaust after-treatment rig.
   - Proposed strategies to study the PM deposition process more rigorously (such as a Lagrangian method and a novel multiphase DNS framework that can resolve all the inherent coupling between the phases.)

2. Development of a novel numerical method that uses a multiphase Direct Numerical Simulation (DNS) technique based on the immersed boundary method to fully resolve the complete particle dynamics (including Brownian dynamics) of particulate aerosols.

   - Proposed a novel Immersed boundary based multiphase DNS framework for the treatment of rarefied particulate aerosols (IB-FSI framework).
   - Extended the applicability of the traditional Ounis and Ahmadi model (3.4) towards this DNS framework by incorporating the fully resolved hydrodynamics within the Langevin description of the particle motion.

- Demonstrated and validated the applicability of this framework to accurately resolve the particle dynamics of spherical soot like particles (in unbounded domains).

- Identified classical results such as exponential tail decay of the velocity auto-correlation function and transition from a ballistic to a diffusive transport regime (that corresponded well with the traditional analytical models of Einstein and Smoluchowski).

- Extended the IB-FSI framework to describe fractal shaped soot aggregate particles (in unbounded domains).

Some limitations

We would also like to emphasize some of the inherent limitations with the novel IB-FSI framework that was developed during the course of this thesis. These can be summarized as follows -

1. The IB-DNS framework can accurately resolve the particulate physics provided the particle-fluid density ratios are sufficiently high (i.e. the Langevin treatment is still valid due to prevalence of quasi-steady hydrodynamic effects)

2. Currently only unbounded flows can be handled (this is because the closures employed in the Langevin description to account for rarefaction are developed for unbounded flows)

3. Similarly, particle-particle interactions are currently not handled as well.

4. The asymmetric rotation of the fractal aggregates still have to be handled correctly. This is currently absent in the framework (although the necessary infrastructure to implement and solve any prescribed rigid body motion is in place).

5. Currently, the results have been extrapolated from only a single (but long) realization of the particle dynamics i.e. we use only a single random seed to initialize our stochastic process. For a more exact description, an ensemble averaging over several stochastic process paths is desired.

Future work

This work has established a very powerful numerical method (i.e. IB-FSI framework) to deal with particulate aerosols. There is however some further scope for the development of this tool. First and foremost, ensemble averaged results from multiple realizations of the Brownian dynamics simulations discussed in this work would need to be collected (in order to conclusively account for the statistical behaviour). The obvious first extension of this work would be to model near wall deposition of particulates (i.e. PM aerosols in a bounded domain). Such an extension would demand a greater insight into near wall rarefaction phenomena. This extension would naturally lead to the next research question i.e. resolution of particle-particle and particle-wall interactions in rarefied flows. As stated earlier, all the necessary infrastructure to account for these effects are already

available in the IB-FSI framework numerically at least, so a detailed investigation into the physics is heavily desired. For such research questions, the more well established molecular methods such as discrete simulation Monte Carlo (DSMC) would provide a more conclusive account of the relevant behaviour, enabling the formulation of simple closures that can be later used in the IB-FSI framework to account for the right physics. The inclusion of these two critical extensions to the framework would potentially enhance its applicability to real world systems even further.

Chapter 6
Summary of papers

6.1 Paper A

6.1.1 Motivation and division of work

This paper aims at highlighting a fundamental knowledge gap in the numerical modelling of particulate aerosols. Modelling PM as inert spheres does not entirely reflect on the real transport and deposition of such particulates. I am a co-author mainly contributing to some of the results and reviewing of the final manuscript. My main contribution consisted of setting up and performing both the experiments and simulations for assessing the capture of inert particulates in a monolith channel. The other authors contributed towards some of the other results presented in the work. Jonas Sjöblom and Henrik Ström co-supervised this work.

6.1.2 Results and discussion

In this paper, we evaluate the deposition of diesel (combustion) generated nano-particles using a combination of experimental and numerical techniques. Successful optimization of any after-treatment device that can control PM emissions relies on the existence of numerical tools to predict the momentum, heat and mass transfer between these types of particles and the surrounding gas phase. We evaluate the need for such tools by highlighting the importance of understanding the transport and deposition of real reactive PM in the channels of a regular mitigation device such as a DPF. It is clearly demonstrated using both experimental and numerical evidence that modelling PM as inert spheres that are trapped by Brownian deposition does not capture the right behaviour (as noted in experiments), meaning that PM are reactive. This is further in-directly confirmed by performing numerical and experimental trials with inert NaCl particulates. The purpose of this is to show that both experiments and simulation correspond well if inert material is studied, and diverge when real reactive PM are studied with models for inert spheres. Further, a conceptual model is proposed that is able to explain the initially observed discrepancies between measurements and simulations, by describing the particulate matter as a mixture of three different types of particles: truly inert particles, semi-volatile particles and completely volatile particles. Hence a clear need for more rigorous tools

that can handle the transport and deposition of reactive particulates is identified (such as multiphase DNS modelling strategies).

6.2   Paper B

Ananda Subramani Kannan, Vasileios Naserentin, Andreas Mark, Dario Maggiolo, Gaetano Sardina, Srdjan Sasic, and Henrik Ström. A novel multiphase DNS method for the resolution of Brownian motion of soot-like particles in a rarefied gas using a continuum framework. *To be submitted to a journal* (2018)

6.2.1   Motivation and division of work

The main objective of this work is to propose a novel multiphase DNS technique based on the immersed boundary method to study the diffusion dynamics of soot aerosols (addressing the need identified in Paper A). Besides being the main author, my contribution consisted of setting up and conceptualizing the simulations, post-processing and analyzing the results. The co-authors supervised and reviewed this work and provided valuable feedback on the analyzed results and on the drafted manuscript.

6.2.2   Results and discussion

In this paper we formulate a novel numerical method that couples the extended Langevin description with a mirroring immersed boundary (IB) method (multiphase DNS). This technique would allow for the inclusion of the resolved fluid flow (around the particle) within the conventional extended Langevin description which generally uses quasi-steady relations to account for the hydrodynamics. We analyse the consequences of resolving Brownian motion in an unbounded domain using this framework and evaluate the diffusion dynamics (mean squared displacements, velocity auto-correlation functions and diffusivities) of a spherical transported particle, in relation to the conventional treatment. The proposed method is able to capture the transition from a particle-inertia dominated (highly correlated) ballistic regime to a non-correlated diffusive one (as given by the Stokes-Einstein relation) and further accurately estimate the resulting diffusivity of a spherical nanoparticle. Moreover, the standard exponential decay of the velocity auto-correlation function (for the Brownian diffusion of heavy particles) is also noted in the simulations of the gas-solid system. Our results show that the proposed model can be used within any multiphase DNS framework to reproduce the meandering motion of soot particles under rarefied conditions. It should however be stressed that this method is valid so long as the Langevin treatment and the Cunningham correction have a basis (i.e. high particle-fluid density ratios and unbounded flows).

References

[1] Mark A., Andersson Bjorn, Tafuri S., Engstrom K., Sorod H., Edelvik F., and Carlson J. S. Simulation of electrostatic rotary bell spray painting in automotive paint shops. *Atomization and Sprays* **23**.1 (2013), 25–45. ISSN: 1044-5110.

[2] M. J. Aftosmis. *Lecture notes: Solution Adaptive Cartesian Grid Methods for Aerodynamic Flows with Complex Geometries.* 1997.

[3] B. J. Alder and T. E. Wainwright. Decay of the Velocity Autocorrelation Function. *Phys. Rev. A* **1** (1 1970), 18–21. DOI: 10.1103/PhysRevA.1.18. URL: https://link.aps.org/doi/10.1103/PhysRevA.1.18.

[4] Michael D. Allen and Otto G. Raabe. Slip Correction Measurements of Spherical Solid Aerosol Particles in an Improved Millikan Apparatus. *Aerosol Science and Technology* **4**.3 (1985), 269–286. ISSN: 0278-6826. DOI: 10.1080/02786828508959055. URL: https://doi.org/10.1080/02786828508959055.

[5] Paul J. Atzberger, Peter R. Kramer, and Charles S. Peskin. A stochastic immersed boundary method for fluid-structure dynamics at microscopic length scales. *Journal of Computational Physics* **224**.2 (2007), 1255–1292. ISSN: 0021-9991. DOI: https://doi.org/10.1016/j.jcp.2006.11.015. URL: http://www.sciencedirect.com/science/article/pii/S0021999106005766.

[6] Robert W. Barber and David R. Emerson. Challenges in Modeling Gas-Phase Flow in Microchannels: From Slip to Transition. *Heat Transfer Engineering* **27**.4 (2006), 3–12. ISSN: 0145-7632. DOI: 10.1080/01457630500522271. URL: https://doi.org/10.1080/01457630500522271.

[7] Robert G. Bartle. Return to the Riemann Integral. *The American Mathematical Monthly* **103**.8 (1996), 625–632. ISSN: 00029890, 19300972. DOI: 10.2307/2974874. URL: http://www.jstor.org/stable/2974874.

[8] J. F. Brady, and G. Bossis. Stokesian Dynamics. *Annual Review of Fluid Mechanics* **20**.1 (1988), 111–157. DOI: 10.1146/annurev.fl.20.010188.000551. URL: https://www.annualreviews.org/doi/abs/10.1146/annurev.fl.20.010188.000551.

[9] Carlo Cercignani. *Rarefied gas dynamics: From basic concepts to actual calcu- lations.* Cambridge university press, 2000. ISBN: 9780521659925.

[10] S. Chandrasekhar. Stochastic Problems in Physics and Astronomy. *Reviews of Modern Physics* **15**.1 (1943), 1–89. DOI: 10.1103/RevModPhys.15.1. URL: https://link.aps.org/doi/10.1103/RevModPhys.15.1.

[11] Stéphane Colin. Rarefaction and compressibility effects on steady and transient gas flows in microchannels. *Microfluidics and Nanofluidics* **1**.3 (2005), 268–279. ISSN: 1613-4990. DOI: 10.1007/s10404-004-0002-y. URL: https://doi.org/10.1007/s10404-004-0002-y.

[12] Ebenezer Cunningham. On the Velocity of Steady Fall of Spherical Particles through Fluid Medium. *Proceedings of the Royal Society of London Series A* **83**.563 (1910), 357–365.

[13] C N Davies. Definitive equations for the fluid resistance of spheres. *Proceedings of the Physical Society* **57**.4 (1945), 259. URL: http://stacks.iop.org/0959-5309/57/i=4/a=301.

[14] G. De Fabritiis, M. Serrano, R. Delgado-Buscalioni, and P. V. Coveney. Fluctuating hydrodynamic modeling of fluids at the nanoscale. *Physical Review E* **75**.2 (2007), 026307. DOI: 10.1103/PhysRevE.75.026307. URL: https://link.aps.org/doi/10.1103/PhysRevE.75.026307.

[15] Steven Delong, Florencio Balboa Usabiaga, Rafael Delgado-Buscalioni, Boyce E. Griffith, and Aleksandar Donev. Brownian dynamics without Green's functions. *The Journal of Chemical Physics* **140**.13 (2014), 134110. ISSN: 0021-9606. DOI: 10.1063/1.4869866. URL: https://doi.org/10.1063/1.4869866.

[16] Directive 2008/50/EC of the European Parliament and of the Council of 21 May 2008 on ambient air quality and cleaner air for Europe. *OJ* **L 152** (2008-06-11), 1–44.

[17] J. P. Van Doormaal and G. D. Raithby. Enhancements of the SIMPLE method for predicting incompressible fluid flows. *Numerical Heat Transfer* **7**.2 (1984), 147–163. DOI: 10.1080/01495728408961817. eprint: https://doi.org/10.1080/01495728408961817. URL: https://doi.org/10.1080/01495728408961817.

[18] Fredrik Edelvik, Andreas Mark, Niklas Karlsson, Tomas Johnson, and Johan S. Carlson. "Math-Based Algorithms and Software for Virtual Product Realization Implemented in Automotive Paint Shops". *Math for the Digital Factory*. Ed. by Luca Ghezzi, Dietmar Hömberg, and Chantal Landry. Cham: Springer International Publishing, 2017, pp. 231–251. ISBN: 978-3-319-63957-4. DOI: 10.1007/978-3-319-63957-4_11. URL: https://doi.org/10.1007/978-3-319-63957-4_11.

[19] Albert Einstein. Über die von der molekularkinetischen Theorie der Wärme geforderte Bewegung von in ruhenden Flüssigkeiten suspendierten Teilchen. *Annalen der Physik* **322**.8 (1905), 549–560. DOI: 10.1002/andp.19053220806.

[20] Donald L. Ermak and J. A. McCammon. Brownian dynamics with hydrodynamic interactions. *The Journal of Chemical Physics* **69**.4 (1978), 1352–1360. ISSN: 0021-9606. DOI: 10.1063/1.436761. URL: https://doi.org/10.1063/1.436761.

[21] P. Español and P. Warren. Statistical Mechanics of Dissipative Particle Dynamics. *EPL (Europhysics Letters)* **30**.4 (1995), 191. ISSN: 0295-5075. URL: http://stacks.iop.org/0295-5075/30/i=4/a=001.

[22] Pep Español. Stochastic differential equations for non-linear hydrodynamics. *Physica A: Statistical Mechanics and its Applications* **248**.1 (1998), 77–96. ISSN: 0378-4371. DOI: https://doi.org/10.1016/S0378-4371(97)00461-5. URL: http://www.sciencedirect.com/science/article/pii/S0378437197004615.

[23] Mohamed Gad-El-Hak. Gas and Liquid Transport at the Microscale. *Heat Transfer Engineering* **27**.4 (2006), 13–29. ISSN: 0145-7632. DOI: 10.1080/01457630500522305. URL: https://doi.org/10.1080/01457630500522305.

[24] Barouch Giechaskiel and Yannis Drossinos. Theoretical Investigation of Volatile Removal Efficiency of Particle Number Measurement Systems. *SAE International Journal of Engines* **3**.1 (2010), 1140–1151. DOI: https://doi.org/10.4271/2010-01-1304. URL: https://doi.org/10.4271/2010-01-1304.

[25] Ranganathan Gopalakrishnan, Thaseem Thajudeen, and Christopher J. Hogan. Collision limited reaction rates for arbitrarily shaped particles across the entire diffusive Knudsen number range. *The Journal of Chemical Physics* **135**.5 (2011),

054302. DOI: 10.1063/1.3617251. eprint: https://doi.org/10.1063/1.3617251. URL: https://doi.org/10.1063/1.3617251.

[26]　Robert D. Groot and Patrick B. Warren. Dissipative particle dynamics: Bridging the gap between atomistic and mesoscopic simulation. *The Journal of Chemical Physics* **107**.11 (1997), 4423–4435. ISSN: 0021-9606. DOI: 10.1063/1.474784. URL: https://doi.org/10.1063/1.474784.

[27]　Johan Göhl, Andreas Mark, Srdjan Sasic, and Fredrik Edelvik. An immersed boundary based dynamic contact angle framework for handling complex surfaces of mixed wettabilities. *International Journal of Multiphase Flow* (2018). ISSN: 0301-9322. DOI: https://doi.org/10.1016/j.ijmultiphaseflow.2018.08.001.

[28]　Johan Göhl, Kajsa Markstedt, Andreas Mark, Karl Håkansson, Paul Gatenholm, and Fredrik Edelvik. Simulations of 3D bioprinting: predicting bioprintability of nanofibrillar inks. *Biofabrication* **10**.3 (2018), 034105. URL: http://stacks.iop.org/1758-5090/10/i=3/a=034105.

[29]　E. H. Hauge and A. Martin-Löf. Fluctuating hydrodynamics and Brownian motion. *Journal of Statistical Physics* **7**.3 (1973), 259–281. ISSN: 1572-9613. DOI: 10.1007/BF01030307. URL: https://doi.org/10.1007/BF01030307.

[30]　E. J. Hinch. Application of the Langevin equation to fluid suspensions. *Journal of Fluid Mechanics* **72**.3 (1975), 499–511. DOI: 10.1017/S0022112075003102.

[31]　Rongxin Huang, Isaac Chavez, Katja M. Taute, Branimir Lukić, Sylvia Jeney, Mark G. Raizen, and Ernst-Ludwig Florin. Direct observation of the full transition from ballistic to diffusive Brownian motion in a liquid. *Nature Physics* **7** (2011), 576. DOI: 10.1038/nphys1953. URL: http://dx.doi.org/10.1038/nphys1953.

[32]　Joseph B. Hubbard and Jack F. Douglas. Hydrodynamic friction of arbitrarily shaped Brownian particles. *Phys. Rev. E* **47** (5 1993), R2983–R2986. DOI: 10.1103/PhysRevE.47.R2983. URL: https://link.aps.org/doi/10.1103/PhysRevE.47.R2983.

[33]　Kiyosi Itô. "STOCHASTIC INTEGRATION". *Vector and Operator Valued Measures and Applications*. Ed. by Don H. Tucker and Hugh B. Maynard. Academic Press, 1973, pp. 141–148. ISBN: 978-0-12-702450-9. DOI: https://doi.org/10.1016/B978-0-12-702450-9.50020-8. URL: http://www.sciencedirect.com/science/article/pii/B9780127024509500208.

[34]　Tomas Johnson, Stefan Jakobsson, Benjamin Wettervik, Björn Andersson, Andreas Mark, and Fredrik Edelvik. A finite volume method for electrostatic three species negative corona discharge simulations with application to externally charged powder bells. *Journal of Electrostatics* **74** (2015), 27 –36. ISSN: 0304-3886. DOI: https://doi.org/10.1016/j.elstat.2014.12.009. URL: http://www.sciencedirect.com/science/article/pii/S0304388614001338.

[35]　Tomas Johnson, Pekka Röyttä, Andreas Mark, and Fredrik Edelvik. Simulation of the spherical orientation probability distribution of paper fibers in an entire suspension using immersed boundary methods. *Journal of Non-Newtonian Fluid Mechanics* **229** (2016), 1 –7. ISSN: 0377-0257. DOI: https://doi.org/10.1016/j.jnnfm.2016.01.001. URL: http://www.sciencedirect.com/science/article/pii/S0377025716000045.

[36] Ananda Subramani Kannan, Vasileios Naserentin, Andreas Mark, Dario Maggiolo, Gaetano Sardina, Srdjan Sasic, and Henrik Ström. A novel multiphase DNS method for the resolution of Brownian motion of soot-like particles in a rarefied gas using a continuum framework. *To be submitted to a journal* (2018).

[37] Ananda Subramani Kannan and Houman Ojagh. Particulate matter removal in automotive aftertreatment systems. *Chalmers university of technology, Master Thesis* (2013). ISSN: 1652-8557.

[38] Em Karniadakis George, Ali Beskok, and Narayan Aluru. *Microflows and Nanoflows: Fundamentals and Simulation.* Vol. 23. Springer-Verlag New York, 2005. DOI: 10.1007/0-387-28676-4.

[39] D.B. Kittelson. Engines and nanoparticles: A review. *Journal of Aerosol Science* **29**.5-6 (1998), 575–588. DOI: 10.1016/S0021-8502(97)10037-4.

[40] Peter R. Kramer, Charles S. Peskin, and Paul J. Atzberger. On the foundations of the stochastic immersed boundary method. *Computer Methods in Applied Mechanics and Engineering* **197**.25 (2008), 2232–2249. ISSN: 0045-7825. DOI: https://doi.org/10.1016/j.cma.2007.11.010. URL: http://www.sciencedirect.com/science/article/pii/S0045782507004641.

[41] Ü Ö Köylü, G. M. Faeth, T. L. Farias, and M. G. Carvalho. Fractal and projected structure properties of soot aggregates. *Combustion and Flame* **100**.4 (1995), 621–633. ISSN: 0010-2180. DOI: https://doi.org/10.1016/0010-2180(94)00147-K. URL: http://www.sciencedirect.com/science/article/pii/001021809400147K.

[42] L. D. Landau and E. M. Lifshitz. "CHAPTER VI - DIFFUSION". *Fluid Mechanics (Second Edition).* Ed. by L. D. Landau and E. M. Lifshitz. Pergamon, 1987, pp. 227–237. ISBN: 978-0-08-033933-7. DOI: https://doi.org/10.1016/B978-0-08-033933-7.50014-3. URL: http://www.sciencedirect.com/science/article/pii/B9780080339337500143.

[43] Paul Langevin. Sur la théorie du mouvement brownien. *C. R. Acad. Sci. (Paris)* **146** (1908), 530–533. DOI: https://doi.org/10.1119/1.18725.

[44] B.P. Leonard. A stable and accurate convective modelling procedure based on quadratic upstream interpolation. *Computer Methods in Applied Mechanics and Engineering* **19**.1 (1979), 59 –98. ISSN: 0045-7825. DOI: https://doi.org/10.1016/0045-7825(79)90034-3. URL: http://www.sciencedirect.com/science/article/pii/0045782579900343.

[45] Z. Gerald Liu, Devin R. Berg, Thaddeus A. Swor, and James J. Schauer. Comparative Analysis on the Effects of Diesel Particulate Filter and Selective Catalytic Reduction Systems on a Wide Spectrum of Chemical Species Emissions. *Environmental Science & Technology* **42**.16 (2008), 6080–6085. DOI: 10.1021/es8004046. eprint: https://doi.org/10.1021/es8004046. URL: https://doi.org/10.1021/es8004046.

[46] P. Worth Longest and Jinxiang Xi. Effectiveness of Direct Lagrangian Tracking Models for Simulating Nanoparticle Deposition in the Upper Airways. *Aerosol Science and Technology* **41**.4 (2007), 380–397. DOI: 10.1080/02786820701203223. eprint: https://doi.org/10.1080/02786820701203223. URL: https://doi.org/10.1080/02786820701203223.

[47] A. Majda and P. Kramer. Stochastic Mode Reduction for the Immersed Boundary Method. *SIAM Journal on Applied Mathematics* **64**.2 (2004), 369–400. ISSN: 0036-1399. DOI: 10.1137/S0036139903422139. URL: https://doi.org/10.1137/S0036139903422139.

[48] M. Malek Mansour, Alejandro L. Garcia, George C. Lie, and Enrico Clementi. Fluctuating hydrodynamics in a dilute gas. *Physical Review Letters* **58**.9 (1987), 874–877. DOI: 10.1103/PhysRevLett.58.874. URL: https://link.aps.org/doi/10.1103/PhysRevLett.58.874.

[49] A. Mark, E. Svenning, and F. Edelvik. An immersed boundary method for simulation of flow with heat transfer. *International Journal of Heat and Mass Transfer* **56**.1 (2013), 424 –435. ISSN: 0017-9310. DOI: https://doi.org/10.1016/j.ijheatmasstransfer.2012.09.010. URL: http://www.sciencedirect.com/science/article/pii/S0017931012007041.

[50] Andreas Mark, R Rundqvist, and Fredrik Edelvik. Comparison Between Different Immersed Boundary Conditions for Simulation of Complex Fluid Flows. *Fluid Dynamics and Materials Processing* **7** (Sept. 2011), 241–258. DOI: 10.3970/fdmp.2011.007.241.

[51] Andreas Mark and Berend G. M. van Wachem. Derivation and validation of a novel implicit second-order accurate immersed boundary method. *Journal of Computational Physics* **227**.13 (2008), 6660–6680. ISSN: 0021-9991. DOI: https://doi.org/10.1016/j.jcp.2008.03.031. URL: http://www.sciencedirect.com/science/article/pii/S0021999108001770.

[52] Martin R. Maxey and James J. Riley. Equation of motion for a small rigid sphere in a nonuniform flow. *The Physics of Fluids* **26**.4 (1983), 883–889. ISSN: 0031-9171. DOI: 10.1063/1.864230. URL: https://aip.scitation.org/doi/abs/10.1063/1.864230.

[53] James Clark Maxwell. On Stresses in Rarified Gases Arising from Inequalities of Temperature. *Philosophical Transactions of the Royal Society of London* **170** (1879), 231–256.

[54] R. A. Millikan. The Isolation of an Ion, a Precision Measurement of its Charge, and the Correction of Stokes's Law. *Phys. Rev. (Series I)* **32** (4 1911), 349–397. DOI: 10.1103/PhysRevSeriesI.32.349. URL: https://link.aps.org/doi/10.1103/PhysRevSeriesI.32.349.

[55] Jean-Pierre Minier and Eric Peirano. The pdf approach to turbulent polydispersed two-phase flows. *Physics Reports* **352**.1 (2001), 1–214. ISSN: 0370-1573. DOI: https://doi.org/10.1016/S0370-1573(01)00011-4. URL: http://www.sciencedirect.com/science/article/pii/S0370157301000114.

[56] Rajat Mittal and Gianluca Iaccarino. Immersed Boundary Methods. *Annual Review of Fluid Mechanics* **37**.1 (2005), 239–261. DOI: 10.1146/annurev.fluid.37.061903.175743. eprint: https://doi.org/10.1146/annurev.fluid.37.061903.175743. URL: https://doi.org/10.1146/annurev.fluid.37.061903.175743.

[57] Abouzar Moshfegh, Mehrzad Shams, Goodarz Ahmadi, and Reza Ebrahimi. A new expression for spherical aerosol drag in slip flow regime. *Journal of Aerosol Science* **41**.4 (2010), 384–400. ISSN: 0021-8502. DOI: https://doi.org/10.1016/

j.jaerosci.2010.01.010. URL: http://www.sciencedirect.com/science/article/pii/S0021850210000200.

[58] *National emissions reported to the Convention on Long-range Transboundary Air Pollution (LRTAP Convention) provided by European Environment Agency (EEA).* Press Release. 2013. URL: https://www.eea.europa.eu/data-and-maps/indicators/emissions-of-primary-particles-and-5/assessment-3.

[59] M. Naumov, M. Arsaev, P. Castonguay, J. Cohen, J. Demouth, J. Eaton, S. Layton, N. Markovskiy, I. Reguly, N. Sakharnykh, V. Sellappan, and R. Strzodka. AmgX: A Library for GPU Accelerated Algebraic Multigrid and Preconditioned Iterative Methods. *SIAM Journal on Scientific Computing* **37**.5 (2015), S602–S626. DOI: 10.1137/140980260. eprint: https://doi.org/10.1137/140980260. URL: https://doi.org/10.1137/140980260.

[60] Nathan M. Newmark. A Method of Computation for Structural Dynamics. *Journal of the Engineering Mechanics Division* **85** (3 1959), 67–94.

[61] Benoît Noetinger. Fluctuating hydrodynamics and Brownian motion. *Physica A: Statistical Mechanics and its Applications* **163**.2 (1990), 545–558. ISSN: 0378-4371. DOI: https://doi.org/10.1016/0378-4371(90)90144-H. URL: http://www.sciencedirect.com/science/article/pii/037843719090144H.

[62] G Okyay. Impact of the morphology of soot aggregates on their radiative properties and the subsequent radiative heat transfer through sooty gaseous mixtures. *PhD Thesis* (2016).

[63] Nada Osseiran and Kimberly Chriscaden. Press Release. 2016. URL: http://www.who.int/news-room/detail/12-05-2016-air-pollution-levels-rising-in-many-of-the-world-s-poorest-cities.

[64] H. Ounis and G. Ahmadi. Analysis of Dispersion of Small Spherical Particles in a Random Velocity Field. *Journal of Fluids Engineering* **112**.1 (1990), 114–120. ISSN: 0098-2202. DOI: 10.1115/1.2909358. URL: http://dx.doi.org/10.1115/1.2909358.

[65] Hadj Ounis and Goodarz Ahmadi. A Comparison of Brownian and Turbulent Diffusion. *Aerosol Science and Technology* **13**.1 (1990), 47–53. ISSN: 0278-6826. DOI: 10.1080/02786829008959423. URL: https://doi.org/10.1080/02786829008959423.

[66] C S Peskin. The Fluid Dynamics of Heart Valves: Experimental, Theoretical, and Computational Methods. *Annual Review of Fluid Mechanics* **14**.1 (1982), 235–259. DOI: 10.1146/annurev.fl.14.010182.001315. eprint: https://doi.org/10.1146/annurev.fl.14.010182.001315. URL: https://doi.org/10.1146/annurev.fl.14.010182.001315.

[67] A. Rahman. Correlations in the Motion of Atoms in Liquid Argon. *Phys. Rev.* **136** (2A 1964), A405–A411. DOI: 10.1103/PhysRev.136.A405. URL: https://link.aps.org/doi/10.1103/PhysRev.136.A405.

[68] C. M. Rhie and W. L. Chow. Numerical study of the turbulent flow past an airfoil with trailing edge separation. *AIAA Journal* **21**.11 (1983), 1525–1532. DOI: 10.2514/3.8284. URL: https://doi.org/10.2514/3.8284.

[69] Steven N. Rogak, Richard C. Flagan, and Hung V. Nguyen. The Mobility and Structure of Aerosol Agglomerates. *Aerosol Science and Technology* **18**.1 (1993),

25–47. DOI: `10.1080/02786829308959582`. eprint: `https://doi.org/10.1080/02786829308959582`. URL: `https://doi.org/10.1080/02786829308959582`.

[70]   Subrata Roy, Reni Raju, Helen F. Chuang, Brett A. Cruden, and M. Meyyappan. Modeling gas flow through microchannels and nanopores. *Journal of Applied Physics* **93**.8 (2003), 4870–4879. ISSN: 0021-8979. DOI: `10.1063/1.1559936`. URL: `https://doi.org/10.1063/1.1559936`.

[71]   Robert Rundqvist, Andreas Mark, Björn Andersson, Anders Ålund, Fredrik Edelvik, Sebastian Tafuri, and Johan S. Carlson. "Simulation of Spray Painting in Automotive Industry". *Numerical Mathematics and Advanced Applications 2009*. Ed. by Gunilla Kreiss, Per Lötstedt, Axel Målqvist, and Maya Neytcheva. Berlin, Heidelberg: Springer Berlin Heidelberg, 2010, pp. 771–779. ISBN: 978-3-642-11795-4.

[72]   J. C. Simo and K. K. Wong. Unconditionally stable algorithms for rigid body dynamics that exactly preserve energy and momentum. *International Journal for Numerical Methods in Engineering* **31**.1 (1991), 19–52. DOI: `10.1002/nme.1620310103`. eprint: `https://onlinelibrary.wiley.com/doi/pdf/10.1002/nme.1620310103`. URL: `https://onlinelibrary.wiley.com/doi/abs/10.1002/nme.1620310103`.

[73]   Jonas Sjöblom, Ananda Subramani Kannan, Houman Ojagh, and Henrik Ström. Modelling of particulate matter transformations and capture efficiency. *The Canadian Journal of Chemical Engineering* **92**.9 (2014), 1542–1551. DOI: `10.1002/cjce.22004`. eprint: `https://onlinelibrary.wiley.com/doi/pdf/10.1002/cjce.22004`. URL: `https://onlinelibrary.wiley.com/doi/abs/10.1002/cjce.22004`.

[74]   Jonas Sjöblom and Henrik Ström. Capture of Automotive Particulate Matter in Open Substrates. *Industrial & Engineering Chemistry Research* **52**.25 (2013), 8373–8385. DOI: `10.1021/ie4004333`. eprint: `https://doi.org/10.1021/ie4004333`. URL: `https://doi.org/10.1021/ie4004333`.

[75]   Krzysztof Skorupski. Software. 2016. URL: `http://www.scattering.eu/`.

[76]   Krzysztof Skorupski, Janusz Mroczka, Thomas Wriedt, and Norbert Riefler. A fast and accurate implementation of tunable algorithms used for generation of fractal-like aggregate models. *Physica A: Statistical Mechanics and its Applications* **404** (2014), 106 –117. ISSN: 0378-4371. DOI: `https://doi.org/10.1016/j.physa.2014.02.072`. URL: `http://www.sciencedirect.com/science/article/pii/S0378437114001812`.

[77]   M. von Smoluchowski. Zur kinetischen Theorie der Brownschen Molekularbewegung und der Suspensionen. *Annalen der Physik* **326**.14 (1906), 756–780. ISSN: 0003-3804. DOI: `10.1002/andp.19063261405`. URL: `https://doi.org/10.1002/andp.19063261405`.

[78]   Gabriel George Stokes. On the Steady Motion of Incompressible Fluids. *Transactions of the Cambridge Philosophical Society* **7** (1848), 439.

[79]   Henrik Ström. Particulate Flows in Aftertreatment Systems. *Chalmers university of technology, PhD Thesis* (2011).

[80]   Henrik Ström, Jonas Sjöblom, Ananda Subramani Kannan, Houman Ojagh, Oskar Sundborg, and Jan Koegler. Near-wall dispersion, deposition and transformation of particles in automotive exhaust gas aftertreatment systems. *International Journal*

of Heat and Fluid Flow **70** (2018), 171 –180. ISSN: 0142-727X. DOI: `https://doi.org/10.1016/j.ijheatfluidflow.2018.02.013`.

[81]   S. Torquato and M. Avellaneda. Diffusion and reaction in heterogeneous media: Pore size distribution, relaxation times, and mean survival time. English (US). *Journal of Chemical Physics* **95**.9 (1991), 6477–6489. ISSN: 0021-9606.

[82]   Laarnie Tumolva, Ji-Yeon Park, Jae suk Kim, Arthur L. Miller, Judith C. Chow, John G. Watson, and Kihong Park. Morphological and Elemental Classification of Freshly Emitted Soot Particles and Atmospheric Ultrafine Particles using the TEM/EDS. *Aerosol Science and Technology* **44**.3 (2010), 202–215. DOI: `10.1080/02786820903518907`. eprint: `https://doi.org/10.1080/02786820903518907`. URL: `https://doi.org/10.1080/02786820903518907`.

[83]   G. E. Uhlenbeck and L. S. Ornstein. On the Theory of the Brownian Motion. *Physical Review* **36**.5 (1930), 823–841. DOI: `10.1103/PhysRev.36.823`. URL: `https://link.aps.org/doi/10.1103/PhysRev.36.823`.

[84]   J. Vom Scheidt. Kloeden, P. E.; Platen, E., Numerical Solution of Stochastic Differential Equations. Berlin etc., Springer-Verlag 1992. XXXVI, 632 pp., 85 figs., DM 118,OO. ISBN 3-540-54062-8 (Applications of Mathematics 23). *ZAMM - Journal of Applied Mathematics and Mechanics / Zeitschrift für Angewandte Mathematik und Mechanik* **74**.8 (1994), 332–332. ISSN: 0044-2267. DOI: `10.1002/zamm.19940740806`. URL: `https://doi.org/10.1002/zamm.19940740806`.

[85]   Benjamin Wettervik, Tomas Johnson, Stefan Jakobsson, Andreas Mark, and Fredrik Edelvik. A domain decomposition method for three species modeling of multi-electrode negative corona discharge – With applications to electrostatic precipitators. *Journal of Electrostatics* **77** (2015), 139 –146. ISSN: 0304-3886. DOI: `https://doi.org/10.1016/j.elstat.2015.08.004`. URL: `http://www.sciencedirect.com/science/article/pii/S0304388615300346`.

[86]   Chonglin Zhang, Thaseem Thajudeen, Carlos Larriba, Thomas E. Schwartzentruber, and Christopher J. Hogan Jr. Determination of the Scalar Friction Factor for Nonspherical Particles and Aggregates Across the Entire Knudsen Number Range by Direct Simulation Monte Carlo (DSMC). *Aerosol Science and Technology* **46**.10 (2012), 1065–1078. DOI: `10.1080/02786826.2012.690543`. eprint: `https://doi.org/10.1080/02786826.2012.69054`. URL: `https://doi.org/10.1080/02786826.2012.690543`.